

ARTICLE PREPRINT

## Towards autonomous photogrammetric forest inventory using a lightweight under-canopy robotic drone

Väinö Karjalainen<sup>a,\*</sup>, Niko Koivumäki<sup>a,\*</sup>, Teemu Hakala<sup>a</sup>, Jesse Muhojoki<sup>a</sup>, Eric Hyypä<sup>a</sup>, Anand George<sup>a</sup>, Juha Suomalainen<sup>a</sup>, Eija Honkavaara<sup>a</sup>

<sup>a</sup>Department of Remote Sensing and Photogrammetry, Finnish Geospatial Research Institute FGI, The National Land Survey of Finland

### ARTICLE HISTORY

Compiled January 22, 2025

### ABSTRACT

Drones are increasingly used in forestry to capture high-resolution remote sensing data. While operations above the forest canopy are already highly automated, flying inside forests remains challenging, primarily relying on manual piloting. Inside dense forests, reliance on the Global Navigation Satellite System (GNSS) for localization is not feasible. Additionally, the drone must autonomously adjust its flight path to avoid collisions. Recently, advancements in robotics have enabled autonomous drone flights in GNSS-denied obstacle-rich areas. In this article, a step towards autonomous forest data collection is taken by building a prototype of a robotic under-canopy drone utilizing state-of-the-art open-source methods and validating its performance for data collection inside forests. The autonomous flight capability was evaluated through multiple test flights in two boreal forest test sites. The tree parameter estimation capability was studied by conducting diameter at breast height (DBH) estimation using onboard stereo camera data and photogrammetric methods. The prototype conducted flights in selected challenging forest environments, and the experiments showed excellent performance in forest reconstruction with a miniaturized stereoscopic photogrammetric system. The stem detection algorithm managed to identify 79.31% of the stems. The DBH estimation had a root mean square error (RMSE) of 3.33 cm (12.79%) and a bias of 1.01 cm (3.87%) across all trees. For trees with a DBH less than 30 cm, the RMSE was 1.16 cm (5.74%), and the bias was 0.13 cm (0.64%). When considering the overall performance in terms of DBH accuracy, autonomy, and forest complexity, the proposed approach was superior compared to methods proposed in the scientific literature. Results provided valuable insights into autonomous forest reconstruction using drones, and several further development topics were proposed.

### KEYWORDS

Robotic; drone; forest; photogrammetry; DBH

## 1. Introduction

Over the last decade, the use of drones in forestry has rapidly increased, offering a practical solution for forest data collection both above and inside the forest canopy (Puliti et al. 2015; Hyypä et al. 2020a; Liang et al. 2019). Modern drones are highly automated and can execute data collection missions highly autonomously in open-air environments using autopilot systems. However, their positioning systems rely exclusively on Global

---

\* Authors contributed equally. CONTACT Väinö Karjalainen. Email: vaino.karjalainen@nls.fi

Navigation Satellite Systems (GNSS) signals, limiting autonomous flights to open areas where these signals are reliable. In dense forests, GNSS localization becomes unreliable due to signal blockages and multipath effects caused by trees (Schubert et al. 2010). Additionally, navigating inside forests requires the capability to autonomously avoid obstacles such as trees and bushes along the flight path. Consequently, under-canopy data collection with drones is still primarily controlled manually by human pilots (e.g. Hyypä et al. 2020a; Liang et al. 2019; Krisanski, Taskhiri, and Turner 2020).

Recent advances in robotics and the enhanced computational capabilities of small embedded computers have enabled drone autonomy even in GNSS-denied, cluttered environments. In recent years, several solutions utilizing various sensor setups and algorithms for autonomous navigation under forest canopies have been proposed (e.g. Liu et al. 2022; Loquercio et al. 2021; Zhou et al. 2022). However, these methods are typically validated by reporting a single test flight in a specific forest environment. Most studies assess the effects of varying object density only in simulators, with only a couple of the methods tested through multiple test flights inside real forests (Loquercio et al. 2021; Ren et al. 2022; Liu, Ren, and Zhang 2024). Therefore, a significant research gap remains regarding the applicability and reliability of these algorithms in diverse forest environments.

The autonomous under-canopy drone solutions proposed in the literature typically focus on aerial robotics and primarily utilize the collected sensor data for navigation. However, recent research has begun to explore boarder applications. For example, Liu et al. (2022) employed a semantic simultaneous localization and mapping (SLAM) algorithm to calculate the number of trees in the explored area. Similarly, Liang et al. (2024) demonstrated the use of autonomous drones for in situ forest observations under the canopy. While their work estimated tree attributes based on data collected during two test flights, it did not evaluate the reliability of autonomous flight itself. Consequently, a research gap remains regarding the boarder application of autonomous drones for forestry applications.

Remote sensing measurements within forests are increasingly used to capture detailed forest information. Terrestrial laser scanning (TLS) made a breakthrough in the early 2000s, followed by the development of various solutions, including static laser scanning using tripods (Bienert et al. 2007) and mobile solutions e.g. handheld devices (Ryding et al. 2015; Bauwens et al. 2016; Marselis et al. 2016; Balenović et al. 2021), backpacks (Liang et al. 2014b, 2018; Hyypä et al. 2020b), ground-based vehicles (Forsman, Holmgren, and Olofsson 2016; Liang et al. 2018; Bienert et al. 2018) or manually operated drones (Chisholm et al. 2013; Brede et al. 2017; Wieser et al. 2017; Hyypä et al. 2020a). Similarly, the use of structure-from-motion (SfM) based point clouds for forest mapping has been demonstrated using different camera solutions (Liang et al. 2014a; Wallace et al. 2016; Kuželka and Surový 2018; Piermattei et al. 2019). Combining these techniques with autonomously navigating drones inside forests represents a highly relevant research opportunity.

To address these gaps and opportunities, this study introduces a novel approach for autonomous data collection and object characterization under unstructured forest canopies. The primary objectives were to assess the performance of an autonomously flying drone in a boreal forest and to demonstrate its capability in measuring tree characteristics. A prototype autonomously flying drone was developed using state-of-the-art open-source algorithms, followed by multiple flight tests to evaluate its performance and suitability for boreal forests. Image data collected by the low-cost onboard stereo-camera was stored for further analysis. The dataset was post-processed using SfM photogrammetry to improve the georeferencing and to generate dense 3D point clouds. Finally, tree

detection and diameter at breast height (DBH) estimation were performed on the point clouds, assessing the potential of the low-cost autonomous system for forest parameter estimation.

The study is structured as follows. Section 2 reviews recent open-source solutions for autonomous drone flights inside forests and state-of-the-art methods forest parameter estimation using drones flying inside forests. Section 3 describes the algorithms, hardware, experiments, and methods for autonomous navigation, tree detection, and DBH estimation. Experimental results are presented in Section 4. Section 5 discusses the results, potential improvements, and concludes the study.

## 2. Related work

### 2.1. *Autonomous flying inside forests*

Autonomous navigation in obstacle-rich environments has been an actively researched topic in robotics during the last decades. Whereas the majority of the research has tried to tackle the 2D path planning problem for autonomous ground vehicles, in recent years increasing number of methods for autonomous path planning and obstacle avoidance have also been published for drones. Although many of the methods proposed in the literature are only tested in simulations or indoor conditions, some of the methods have been also successfully flight-tested inside forests. Some of the authors have also open-sourced their methods to encourage the development of the field. In this section, recent open-source methods successfully flight-tested inside a forest are summarized.

Campos-Macías et al. (2021) proposed a solution that focuses on computational efficiency that can be run in real time with a low-power CPU. The solution used a stereo tracking camera to run Visual-Inertial Odometry (VIO) for pose estimation and a point cloud from an active stereo depth camera to create a 3D voxel map. Collision-free trajectories were planned to the free regions on the map. In addition to multiple indoor environments, the system was tested in a sparse mixed forest. However, the flight distance in the forest test was only 11.58 m.

Liu et al. (2022) proposed a method that aims at large-scale autonomous flights in forest environments. The proposed system used an inertial measurement unit (IMU) and a stereo camera to run VIO and 3D light detection and ranging (LiDAR) to run a semantic simultaneous localization and mapping (SLAM) algorithm. Semantic SLAM was developed to correct drift in the VIO estimate. The system was reported to fly an 800 m long autonomous flight, but the semantic SLAM algorithm was only tested in manual flight. The documented flight tests were performed in a North American pine forest. The forest was relatively dense, but it had a minimal amount of low branches and understory vegetation.

Ren et al. (2022) proposed another LiDAR-based method that generates sphere-shaped safe flight corridors from the point clouds. The method was targeting for high-speed flying in unknown environments. FAST-LIO2 (Xu et al. 2022) was utilized in the pose estimation. In total, 12 test flights with varying flight speeds were performed in a sparse Chinese deciduous forest. The maximum flight speed was 13.7 m/s and 11 of 12 test flights were successful, but the trajectory lengths were not reported. Liu, Ren, and Zhang (2024) have also proposed another method for the same LiDAR-based platform targeting especially safe navigation in the presence of dynamic obstacles and external disturbances with an integrated planning and control framework. Planning was performed within a local grid map and FAST-LIO2 (Xu et al. 2022) was utilized in the

pose estimation. In addition to indoor environments, the system was also tested with 10 successful flights at varying speeds in the same forest as (Ren et al. 2022). The maximum flight speed was 5.86 m/s, and the reported trajectory length was 58.64 m.

Instead of using a single drone, the solution proposed by Ahmad et al. (2022) focused on the navigation of drone swarms. The proposed approach is fully decentralized and tries to mimic the collective navigation behavior of natural flocks and swarms. The physical drone hardware used in the tests incorporated a LiDAR for running the SLAM algorithm by Kohlbrecher et al. (2011), a laser rangefinder as an altimeter, and an Ultra Violet Direction And Ranging (UVDAR) system for relative localization between the drones of the swarm. The approach was tested in a swarm flight inside a forest, but the test forest was very clean containing no low branches or understory vegetation. The flight distance was approximately 40 m.

Zhou et al. (2022) also proposed a solution concentrating on swarm flights. In the proposed solution the drones use VIO for localization and probabilistic maps for obstacle avoidance. Swarm members also share their trajectories over a wireless network and correct the VIO drift based on the relative distances between the drones measured with Ultra Wide Band (UWB) sensors. The proposed solution was tested with palm-sized drones which used only one stereo camera to run both mapping and VIO. In the flight tests, a swarm of drones was successfully flying approximately 80 m through a dense bamboo forest.

The solution proposed by Loquercio et al. (2021) replaced different sensing, mapping, and planning subtasks with a single neural network directly mapping depth images and a pose estimate from VIO to a feasible collision-free trajectory for the drone. The system was trained entirely with simulated data, and the scope of the research was high-speed autonomous flying. Real-world flight tests were performed with a drone using an active stereo depth camera to produce the depth images, and a stereo tracking camera to run VIO. Flight tests were performed in various environments containing also Central-European mixed forests. The forest densities were not reported, but the forests were relatively sparse with a low amount of understory vegetation. The evaluated trajectories were a 40 m long straight line and a circle with a 6 m radius, and multiple test flights were conducted with flight speeds varying from 3 to 10 m/s. The flight success rate was 100 % with a flight speed of 3 m/s and 5 m/s, 80 % with a flight speed of 7 m/s, and 60 % with a flight speed of 10 m/s

Nguyen et al. (2023) proposed also a deep-learning-based method that utilizes neural networks to directly map depth images and partial pose estimates of the drone to a series of actions leading to a collision-free trajectory. The proposed system was also trained entirely in a simulator. In addition to the indoor flight tests, the performance assessment was reported for a single 60 m long trajectory through a dense Finnish pinewood forest making the test environment the most similar to the target environments in this study.

## **2.2. *DBH estimation from under-canopy drone data***

In a forest inventory, DBH is one of the most important tree attributes to be estimated since it provides a measure for the size of a tree and also enables the prediction of the total stem volume (Laasasenaho 1982). During the past decade, photogrammetric systems producing SfM point clouds have been suggested to provide an efficient, low-cost alternative to traditional field measurements of tree attributes, such as DBH. Even though several studies have investigated terrestrial photogrammetric systems (e.g., Liang et al. (2014a); Surovỳ, Yoshimoto, and Panagiotidis (2016); Mokroš et al. (2018); Piermattei

et al. (2019); Xu, Shen, and Cao (2023)) and above-canopy photogrammetric systems (e.g., Wallace et al. (2016); Ye, van Leeuwen, and Nyktas (2019)) for tree attribute estimation, only relatively few studies have tested the use of under-canopy drone systems for the collection of SfM point clouds enabling tree attribute measurements (Kuželka and Surovỳ 2018; Krisanski, Taskhiri, and Turner 2020; Shimabuku, Konoshima, and Ota 2023). If the operation of such under-canopy drone systems can be automated in the future, they would provide a truly efficient solution for the acquisition of accurate forest data.

Kuželka and Surovỳ (2018) manually operated a drone system based on a DJI Phantom 4 Pro within two forest plots to produce low-noise photogrammetric point clouds, from which the DBH of individual trees could be estimated with an RMSE between 2.6 cm and 5.3 cm depending on the plot and the applied analysis method. The studied plots were sparse with only 270-290 trees/ha. Krisanski, Taskhiri, and Turner (2020) performed manual flights of a drone system inside two forest plots with a stem density of approximately 1000 trees/ha to acquire high-density SfM point cloud data, from which the DBH of individual trees could be measured with a RMSE of 1.1-2.1 cm. Shimabuku, Konoshima, and Ota (2023) achieved an RMSE of 0.4-0.7 cm for DBH estimation on two small forest plots using SfM point clouds acquired with an under-canopy flying drone system. The drone system was able to detect obstacles in the horizontal direction, but needed manual piloting to avoid obstacles in the vertical direction and to guide the drone back to the intended flight path after automatic obstacle avoidance in the horizontal direction. They also demonstrated stem volume estimates of individual trees with a RMSE of 15.8-17.2%.

In addition to photogrammetric approaches, LiDAR-based methods have been studied extensively for the purpose of efficiently and accurately estimating various tree attributes, such as DBH, tree height and stem volume. To date, several LiDAR-based mobile platforms have been shown to enable DBH estimation of individual trees with an RMSE of 1-2 cm (Ryding et al. 2015; Bauwens et al. 2016; Cabo et al. 2018; Chen et al. 2019; Hyyppä et al. 2020b,a, 2022), though most studies have focused on relatively sparse forests with little understory vegetation. Even though a LiDAR can be mounted to a variety of other mobile platforms besides a drone, the focus is on the use of under-canopy drones for DBH estimation in this brief literature review.

Chisholm et al. (2013) were the first to demonstrate DBH measurements from point cloud data collected with a manually-piloted drone flying under the forest canopy. They detected 12 trees in the vicinity of the drone trajectory and reported a RMSE of 25.1% for the DBH estimates of the detected trees.

Hyyppä et al. (2020a) collected high-quality point cloud data using a Kaarta Stencil-1 laser scanner mounted horizontally at the bottom of a manually-piloted drone. They demonstrated DBH estimates with a RMSE of 0.6-0.9 cm (2%-3%) on two plots of varying complexity in a boreal forest with a tree density of 410-420 trees/ha. Importantly, their stem diameter estimation algorithm utilized the temporal order of data points to detect stem arcs, thus mitigating distortions caused by slow temporal drifts of the drone trajectory. As the laser scanner was mounted horizontally in their study, the limited field of view made it difficult to obtain direct measurements of tree height. In a follow-up study by Hyyppä et al. (2021), this issue was resolved by instead integrating a rotating laser scanner to an under-canopy flying drone, which resulted in accurate measurements for both stem diameter and tree height. Wang et al. (2021) combined data from above- and under-canopy flights of a manually-piloted drone, resulting in an RMSE of 7.95 cm (33.35%) and a bias of 3.72 cm (15.61%) for the DBH.

Muhojoki et al. (2024) compared the accuracy of the estimated tree attributes from

several LiDAR-based mobile systems, including two under-canopy drone systems, a system by Hovermap (2020 version, Emesent, Milton, Australia) equipped with a Velodyne VLP-16 laser scanner (Velodyne Lidar, San Jose, CA, USA) and a system by Deep Forestry (Deep Forestry, Uppsala, Sweden) utilizing an Ouster OS0-32 Rev. 5 laser scanner (Ouster, San Francisco, CA, USA). Both drones were flown manually in Muhojoki et al. (2024) to collect data in sparse density forest plots. The RMSE and bias of DBH estimates for the Deep Forestry’s and Hovermap’s drones, with bias removal method introduced by Muhojoki et al. (2024), averaged RMSE of 1.5 cm (6.7 %) and bias of -0.7 cm (3.0 %) and RMSE of 1.6 cm (6.9 %) and bias of -0.1 cm (-0.6 %), respectively. Without using bias removal method, RMSE and bias for both drones were significantly higher. Muhojoki et al. (2024) also demonstrated that the under-canopy drone systems can provide roughly as accurate tree attributes as other under-canopy MLS methods, such as handheld LiDARs.

Recently, Liang et al. (2024) applied an autonomously operated under-canopy drone system to collect laser scanning data inside a 50 m × 30 m forest plot with a tree density of approximately 1000 trees/ha. To enable the autonomous flight, a predefined global path was planned, to which the drone system performed real-time adjustments during the flight according to real-time environment conditions. When the flight path covered most of the test plot, they achieved an RMSE of 5.1 cm for the DBH of individual trees, and a similar RMSE for the stem curve.

In addition to under-canopy flying drones, LiDARs have also been integrated to above-canopy flying drones capable of direct stem diameter measurements, though typically with a significantly higher RMSE and a lower tree detection rate due to the larger measurement distance and the upper canopy obstructing the tree stems (Wieser et al. 2017; Brede et al. 2017; Kuželka, Slavík, and Surový 2020; Vandendaele et al. 2021; Feng et al. 2022).

A summary of relevant studies on under canopy forest inventory studies is presented in Table 1.

Table 1.: Accuracy of the stem diameter breast height (DBH) estimations in other studies. SfM-MVS: Structure-from-motion and multi-view stereo; ULS: Under canopy laser scanning; ALS: Above canopy laser scanning. \*averaged values from three plots

Dataset	Type	Number of trees	RMSE (cm)	RMSE%	Bias (cm)	Bias%
Shimabuku et al. (2023) plot I	Drone SfM-MVS	7	0.4	3.2	-	-
Shimabuku et al. (2023) plot II	Drone SfM-MVS	18	0.7	3.6	-	-
Kuželka and Surový (2018)	Drone SfM-MVS	119	2.63-5.31	7.01-13.3	0.27-3.77	0.69-10.11
Krisanski et al. (2020)	Drone SfM-MVS	29	4.1	-	-	-
Liang et al. (2024) traj. I	ULS	143	9.43	63.41	7.17	48.21
Liang et al. (2024) traj. II	ULS	143	4.48	21.37	5.01	14.91
Hyppä et al. (2020a) plot I	ULS	42	0.6	2.3	0.34	1.3
Hyppä et al. (2020a) plot II	ULS	43	1.1	3.5	0.12	0.4
Wang et al. (2021)	ULS&ALS	-	7.95	33.35	3.72	15.61
Muhojoki et al.* (2024)	ULS	50	1.50-1.60	6.70-6.90	0.10-0.70	0.60-3.00

### 3. Materials and methods

#### 3.1. Autonomous navigation algorithms

In this study, the objective was to develop a prototype drone capable of autonomously avoiding obstacles under the forest canopy and operating without GNSS. The drone was required to autonomously fly from the takeoff location to a specified goal point while recording sensor data during the flight. This prototype will later serve as a development platform for more extended and sophisticated data collection tasks.

Among the open-source solutions presented in Section 2.1, the solution by Zhou et al. (2022) was chosen as the base of the prototype. The solution was proven to work with only one stereo camera making it possible to build a smaller and lighter platform. Furthermore, cameras are typically lighter and more power-efficient than LiDARs (Reddy Cenkeramaddi et al. 2020) making them an attractive solution for small under-canopy drones, for which the weight and battery consumption must be optimized. This enables building a compact system that is capable of operating in dense forests.

The main details of the algorithms used in the chosen solution are described briefly in the following and the complete system architecture of the prototype is presented in Figure 1. For more detailed information the readers are referred to the cited original sources.

##### 3.1.1. EGO-Planner-v2

The source code of the planner algorithm by Zhou et al. (2022) was named in Github as EGO-Planner-v2 (ZJU FAST Lab Team 2022a). Even though the EGO-Planner-v2 is designed for swarm flying, in this study, only a single drone system was used. The planner is running on top of the Robot Operating System (ROS) (Quigley et al. 2009). The mapping of EGO-Planner-v2 is based on probabilistic occupancy grid maps (Moravec and Elfes 1985). The mapping module uses depth images as an input and the system adopts the fixed-sized circular buffers proposed by Usenko et al. (2017) for maintaining the local map. The maps also have a virtual floor and a virtual ceiling defining the minimum and maximum altitudes of the grid map respectively. Virtual floor and virtual ceiling restrict the altitude where the algorithm is allowed to plan paths.

In the trajectory planning, EGO-Planner-v2 uses a MINCO (minimum control) (Wang et al. 2022) trajectory representation designed for differentially flat systems, such as quadrotors (Mellinger and Kumar 2011). Planned trajectories are represented as piece-wise polynomial splines with decoupled temporal and spatial parameters (Zhou et al. 2022). The trajectories are optimized iteratively by minimizing the weighted sum of metrics defined for trajectory smoothness and flying time. The feasibility of the planned trajectory is forced by deforming the shape to avoid obstacles and by restricting the magnitudes of trajectory velocity, acceleration, and jerk to fulfill the dynamical constraints of the drone. For computational efficiency, the trajectory constraints are enforced via integrals of penalty functions with large penalty weights, and the integrals are evaluated by a finite sum of equally spaced samples along the timeline. In a simplified form, the optimization of time-dependent objectives  $J$  in one piece of the trajectory can be represented by

$$\min \sum_x \lambda_x J_x \tag{1}$$

where where  $J_x$  are the penalty terms and  $\lambda_x$  are the corresponding weights. Subscripts  $x = \{s, t, d, o, u\}$  stand for the trajectory smoothness, total flying time, dynamical feasibility, obstacle avoidance, and the uniform distribution of constraint evaluation points along the trajectory, respectively. In addition to the above mentioned penalty terms, EGO-Planner-v2 includes also penalty terms for the swarm operations, but those are omitted here. A\* is utilized as the global path-searching algorithm given as an input for the optimization algorithm.

The trajectory planning is continuously performed within a defined local planning distance towards a user-defined global goal until the goal is reached. Since the safety constraints are modeled as integrals in the penalty functions, the feasibility of the trajectory needs to be verified with a post-check after planning (Zhou et al. 2022). Due to the non-static probabilistic map, the post-check after trajectory planning guarantees feasibility only at a certain moment. Hence, a collision-check process is continuously running in the background. If that process detects a potential collision, a trajectory replanning is activated immediately. If the replanning fails and the predicted time to collision is under a given threshold, the planner performs an emergency stop. After the drone has stopped, the trajectory planner tries to start up again and find a new feasible trajectory.

### 3.1.2. VINS-Fusion

The VIO algorithm used by Zhou et al. (2022) was VINS-Fusion (Qin, Li, and Shen 2018; Qin et al. 2019b)(VINS stands for "Visual-Inertial system"), which used grayscale stereo images and IMU data to track the position and orientation of the drone.

VINS-Fusion detects Shi-Tomasi corner features (Shi and Tomasi 1994), and the features are tracked between frames with Kanade-Lucas-Tomasi (KLT) Tracker (Lucas and Kanade 1981). IMU data is used for preintegration, i.e. position, velocity, and orientation are integrated from IMU measurements between two frames. The state optimization is performed within a sliding window including the position, velocity, rotation, and IMU biases. To reduce the computational complexity, old measurements are marginalized into a prior of the estimation process. Certain frames are also selected as keyframes which are saved to a global pose graph after being marginalized out from the sliding window. Keyframes are selected based on the number of tracked features and the average parallax between the features in the newest frame and the latest keyframe.

VINS-Fusion supports loop detection-based relocalization and global pose graph optimization to reduce the accumulated drift in the pose estimate. The loops are detected by storing additional corner features as BRIEF descriptors (Calonder et al. 2010) to DBoW2 (Galvez-López and Tardos 2012) bag-of-word database. After a loop detection, the relocalization process aligns the latest window to past poses and optimizes it utilizing also the feature correspondences with past poses. In addition to sliding window relocalization, also the global pose graph is optimized after loop detections to enforce the global consistency of the poses. Since the roll and pitch angle estimates are drift accumulation-free due to full observability from the gravity measurement of the IMU, the pose graph optimization is performed in 4 degrees of freedom.

VINS-Fusion also adopts an online temporal calibration method for inertial and visual measurements (Qin and Shen 2018). The method can be used for adjusting the time offset  $t_d$  between the camera and the IMU online.

In the swarm operations of the original article (Zhou et al. 2022), the drones used also relative distances measured with Ultra Wide Band (UWB) sensors to correct the drift in the pose estimate of VINS-Fusion. However, with a single drone of this study

that function is omitted.

The parameters used in the configuration of VINS-Fusion were chosen so that the real-time performance was guaranteed. In the initial tests, the IMU noise values used during the calibration were over-optimistic for VINS-Fusion causing instability to the estimates, so the IMU noise values were increased more. All VINS-Fusion configuration parameters are listed in Table 2.

Table 2.: VINS-Fusion parameters.

Parameter	Value
Image resolution	$640 \times 360$
Max number of tracked features	150
Min distance between features	40 px
RANSAC threshold	1 px
Max solver iteration time	0.04 ms
Max solver iterations	8
Keyframe parallax threshold	10 px
Accelerometer noise SD	0.2
Gyroscope noise SD	0.05
Accelerometer random walk SD	0.002
Gyroscope random walk SD	0.0005

### 3.1.3. Tracking controller

The original EGO-Planner-v2 article (Zhou et al. 2022) did not specify the utilized method for trajectory tracking. In this study, an open-source tracking controller (ZJU FAST Lab Team 2022b) by Zhejiang University was used. The tracking controller gets setpoints for position, velocity, acceleration, and yaw from the trajectory planner, and converts those to attitude and thrust setpoint. The setpoints are forwarded to PX4 flight controller software (PX4 Community 2023) responsible for low level attitude and angular rate controls.

## 3.2. Drone hardware

In the physical robot drone prototype, an onboard computer NVIDIA Jetson Orin NX (Santa Clara, California, USA) was used. The used PX4-compliant autopilot was Holybro Kakute H7 (Hongkong, China), which contained also the IMU. The navigation algorithms mentioned in the previous subsection ran on top of the ROS, and the Mavros-protocol was used for communication between the onboard computer and the autopilot. As a camera, Intel RealSense D435 (Intel Realsense Development Team 2023)(Keselman et al. 2017) was used. The camera was capturing both depth images for 3D mapping and grayscale stereo images for VIO.

RealSense D435 is based on active stereoscopy and the camera has an infrared laser projector emitting dots that can be used for triangulation by stereo camera. This can improve the triangulation in low-light conditions and to homogeneous surfaces that contain no features. However, the dots of the laser emitter cause problems for VIO since they are moving with the camera. In the previous setup described by (Karjalainen et al. 2023), a modified version of ROS-RealSense driver was used by Zhou et al. (2021b)

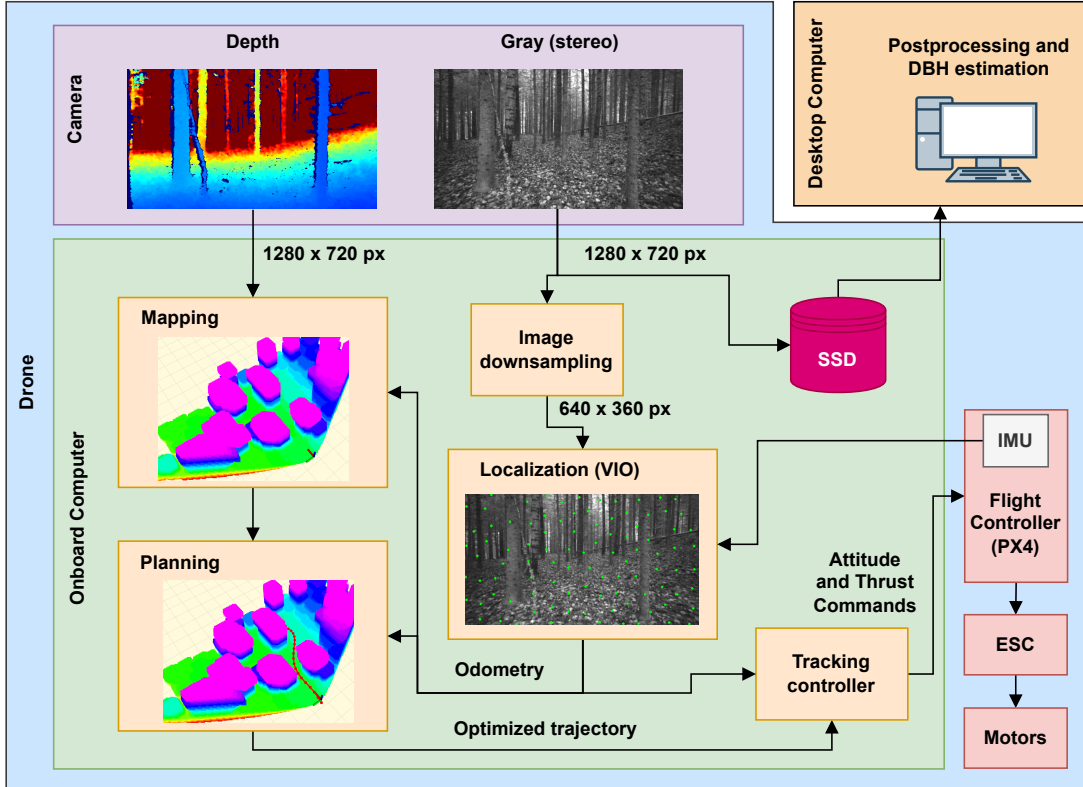


Figure 1.: The system architecture used in the data collection. In comparison to the original EGO-Planner-v2 article by Zhou et al. (2022), UWB-based Drift correction and Wireless trajectory broadcast network modules used for swarm navigation were omitted in this study. Stereo images were downsampled for VIO to guarantee real-time estimation. Full-resolution stereo images were also saved and post-processed to point clouds used in the DBH estimation.

that turns the laser emitter of the camera constantly on and off making it possible to produce high-quality depth images in every other frame, and stereo images without the laser dots in every other frame. However, this solution comes with the drawback of halving the output frame rate of the camera.

In the first test flights described by (Karjalainen et al. 2023), difficulties were encountered in detecting small branches with a depth camera resolution of  $640 \times 480$ , leading to the decision to increase the depth camera resolution to a maximum value of  $1280 \times 720$ . Stereo images for VIO were downsampled to resolution of  $640 \times 360$  to ensure real-time performance. As the maximum frame rate of D435 at a resolution of  $1280 \times 720$  is 30 Hz, the modified driver version would have resulted in a low frame rate of 15 Hz. To ensure the VIO performance in quick turns, the frame rate of 30 Hz was preferred, and hence disabled the IR emitter making the camera function as a passive IR stereo camera. The choice can be further justified with the fact that the usefulness of the IR emitter in forest conditions is questionable, since sunlight contains infrared light that can interfere with the emitted artificial features (Kuan, Ee, and Wei 2019), and the forests typically do not contain large homogeneous surfaces. The Realsense D435 onboard camera was configured to use the builtin automatic exposure control.

The camera-IMU system was calibrated with an open-source camera calibration

toolbox, kalibr (Furgale, Barfoot, and Sibley 2012)(Furgale, Rehder, and Siegwart 2013)(Maye, Furgale, and Siegwart 2013). In the calibration, the intrinsic and extrinsic parameters of the left and right grayscale cameras and the time shift between the camera and the autopilot IMU were calculated from recorded data where Aprilgrid (Olson 2011) was used as a calibration target. The IMU noise parameters needed for the calibration were first obtained with open source tool Allan Variance ROS (Oxford Dynamic Robot Systems Group 2022), and the obtained values were multiplied with 10 before the calibration as suggested in the project wiki of kalibr (ETH Zürich Autonomous Systems Lab 2023).

The computer, the camera, and the autopilot were attached to a 330 mm drone frame. The propellers had two pieces of 6 cm long blades each. The measured weight of the drone including the motors and the onboard computer was 791 g without the batteries, and 1153 g with the batteries. An overview of the used drone hardware is presented in Figure 2.



Figure 2.: The drone hardware used in the flight tests with a forward-facing Realsense D435 camera. Nvidia Jetson Orin NX onboard computer is hidden in the case under the drone frame. Holybro Kakute H7 Flight controller unit is located inside the frame. Batteries (not visible in the picture) are mounted on the top of the drone frame.

### 3.3. Test sites

The performance of the system was evaluated in three different Boreal forest areas. The flight tests of the system were performed in two test areas located in Evo, Finland (61.19°N, 25.11°E). The flight paths went through well-documented forest sample plots that have been widely used in previous studies, such as in Liang et al. (2018, 2019); Wang et al. (2019); Hyypä et al. (2020a,c), and are classified into three complexity categories, i.e., “easy”, “medium”, and “difficult” based on, mainly tree density and amount of the understory vegetation in the plots.

The first plot has been classified as “medium”, and the second one has been classified as “difficult”. The medium difficulty plot had a tree density of 650 trees/ha and a mean

diameter at breast height (DBH) of 28 cm. The most common tree species in the plot were Norway spruce (*Picea abies* (L.) H.Karst.)(81.2%) and Scots pine (*Pinus sylvestris* L.)(9.4%). The difficult forest had a tree density of 2000 trees/ha and a mean DBH of 17 cm. The most common tree species in the plot were Norway spruce (64.4%) and aspen (*Populus tremula*, L.) (18.3%). Only trees with a DBH greater than 5 cm were included in these statistics. From now on, these two test areas are called "Evo-medium" and "Evo-difficult", respectively.

For georeferencing purposes, circular coded targets provided by Agisoft Meatahsape (Agisoft LLC, St. Petersburg, Russia) were placed within the forest plots. The targets had a diameter of 24.7 cm, and the middle dots had a size of 7 cm. Relative distances between the coded targets were measured with Leica Nova TS60 total station with a precision of approximately 2mm (Leica Geosystems 2020). Figure 5 shows coded targets in "Evo-difficult" forest during the test flights.

The third test area was a spruce forest in Paloheinä, Finland (60.26°N, 24.92°E). Aim of the experiment there was to test the loop detection performance of VINS-Fusion by walking with the drone in an environment without coded targets. Estimated average tree density in the area was approximately 2000 trees/ha.



Figure 3.: View from the first takeoff location in the Evo-medium test area. The takeoff location was changed after five test flights.



Figure 4.: View from the takeoff location in the Evo-difficult test forest

### 3.4. *Flight tests*

Test flights in Evo were conducted on 18th October, 2023. Multiple test flights were performed to evaluate the forest-type effects on the performance of autonomous navigation. In total, seven test flights were conducted in the "Evo-medium" test area and nine test flights in the "Evo-difficult" test area. In each test environment, either the takeoff location or the takeoff heading was altered during the test flight campaign to force the drone to follow different paths. In the "Evo-medium" test area, the takeoff location was changed after five test flights. In the "Evo-difficult" test area the takeoff heading was changed after six test flights. The target flight velocity was 1 m/s in all flight tests. The goal was set 36 m forward in the first takeoff location in the "Evo-medium" test area, 34 m forward in the second takeoff location in the "Evo-medium" test area, and 42 m forward in the takeoff location in the "Evo-difficult" test area. The maximum flight height was set to 2.25 m relative to the takeoff location in the "Evo-medium" test area. For the first test flight in the "Evo-difficult" test area, the maximum flight height was set to 2.5 m with respect to the takeoff location and was increased to 2.75 m for the rest of the flights.

The campaign to evaluate the loop detection capability took place on 26th January 2024. Stereo images and IMU data were collected during two walks inside the forest while carrying the drone by hand. The paths of the walks were approximately 340 m and 240 m long, each containing multiple loops where the same scene was observed multiple times. The data collection took place during winter, with the forest covered in snow.



Figure 5.: Control targets for reference trajectory generation in "Evo-difficult" forest. Targets were spread widely to the test site to increase the probability that there would be targets visible in the recorded camera data regardless the path that the robot takes.

### 3.5. *Structure-from-Motion Multi-View Stereo based reconstruction*

Photogrammetric Structure-from-Motion Multi-View Stereo (SfM-MVS) processing was conducted in post-processing mode to generate 3D point clouds for DBH estimation and to generate reference trajectories for evaluating VIO performance.

Stereo image processing was carried out using Agisoft Metashape software (Agisoft LLC, St. Petersburg, Russia) (Metashape Development Team 2021) following similar processing steps as introduced by Viljanen et al. (2018). Every sixth stereo pair were used in the Metashape processing with a stereo baseline of 5 cm and an accuracy setting of  $\pm 0.0015$  m. In the image orientation processing, quality setting was set to high meaning that two times downsampled images were used; the settings for number of key points and tie points per image were 40,000 and 4,000, respectively. To enhance the quality of the post-processed reference trajectories, ground control points (GCPs) were used in the processing with an accuracy setting of  $\pm 0.005$  m. Automatic outlier removal was performed using gradual selection tools of the software based on re-projection error, reconstruction uncertainty, and projection accuracy. Subsequently, a bundle-adjustment was carried out, involving optimization of the sparse point cloud along with the interior (IOP) and the exterior orientation parameters (EOP). Following that, a dense point cloud was calculated using the highest quality setting and mild depth filtering. Finally, the EOPs and dense point clouds were exported.

Point clouds were derived using datasets from four flights conducted in the "Evo-

medium” test area, each designated as follows: I: the first flight, II: the second flight, III: the third flight, IV: the fourth flight, and I-IV: combined processing of all four flights (Combined). The processing was carried out using all GCPs. Additionally, to evaluate the impacts of GCPs, point clouds were generated from the first flight trajectory processed with different GCP configurations, denoted as:  $I_{0GCP}$ : no GCPs,  $I_{1GCP}$ : one GCP at the beginning of the trajectory,  $I_{2GCP}$ : two GCPs, one at the beginning and one at the end of the trajectory, and  $I_{3GCP}$ : three GCPs, positioned at the beginning, middle, and end of the trajectory.

The experiments were conducted in dense forests, where collecting reference data using GNSS was not possible due to the forest canopy blocking the signal. Reference trajectories were generated for the flights using SfM processing. In each case, the reference trajectory was derived from the first takeoff heading and orientation in both Evo test environments.

### 3.6. *Tree parameter estimation*

In this study, trees were detected and their DBHs estimated using an automatic stem diameter estimation algorithm originally proposed by Hyyppä et al. (2020b), and further developed by Hyyppä et al. (2020a) to be suitable for a larger variety of point clouds, including photogrammetric point clouds, and point clouds produced with 3D mobile laser scanners and TLS. The method described by Hyyppä et al. (2020a) was applied to estimate the DBH from point clouds collected with the drone and a TLS system, the latter of which provided reference measurements of DBH (see details in Section 3.7).

The point cloud was first segmented into 40-cm-tall (20-cm-tall for TLS) vertical segments, and 5-s-long temporal segments. The temporal segmentation was done to mitigate point cloud distortions caused by potential slowly-accumulating positioning errors of the moving drone system, and thus the temporal segmentation was not performed for the TLS data. The points potentially corresponding to the tree stems were detected by clustering the points with density-based clustering (DBSCAN, (Ester et al. 1996)), and filtered by fitting a circle to each cluster while accepting only those clusters satisfying the following heuristic criteria: the cluster contained more than 35 points and at least 80 % of the points within 30 mm of the circular arc, the fitted circle radius was between 4 cm and 40 cm, and the points covered at least a 60° central angle of the fitted circle. The accepted clusters were further grouped into tree stems by applying DBSCAN for the center points of the clusters, and the growth direction of each tree was estimated with principal component analysis (PCA). The points within accepted clusters were projected into the plane perpendicular to the growth direction for the final diameter estimation. The diameters were processed into a stem curve by automatically removing clear outliers followed by fitting a smoothing spline to the remaining diameter estimates as a function of height. Finally, the DBH estimates were calculated by interpolating the stem curve at the height of 1.3 m above the ground. For a detailed description of the method, the reader is referred to Hyyppä et al. (2020b,a).

### 3.7. *Performance assessment*

#### 3.7.1. *Autonomous flying performance*

The performance and reliability of the autonomous navigation of the prototype were evaluated based on two factors: the reliability of the obstacle avoidance and the accuracy

of the VIO localization.

Obstacle avoidance reliability was evaluated based on the mission success. A mission was considered successful if the drone reached the end of the flight without major collisions. Minor touches to thin vegetation or branches were allowed, if the drone was able to continue the mission after that. If the given goal was inside an obstacle, the mission was considered successful if the drone managed to fly next to the goal. In addition to obstacle avoidance, the smoothness of the trajectory was assessed. The trajectory was considered smooth if the system did not perform any emergency stops during the flight.

The accuracy of the VIO localization was assessed by calculating the Absolute Trajectory Error (ATE), as proposed by Sturm et al. (2012), with respect to the SfM reference trajectories. In this study, ATE was calculated only for the position estimate, and the error in the orientation estimate was not evaluated. ATE was calculated using the trajectory evaluation toolbox by Zhang and Scaramuzza (2018), which aligns the trajectory estimates with the reference trajectories with the method by Umeyama (1991). The root mean square error (RMSE) of the individual state errors is then calculated to generate a single metric value representing the entire trajectory’s accuracy.. In the mathematical form the error can be presented as

$$\text{ATE}_{\text{pos}} = \left( \frac{1}{N} \sum_{i=0}^{N-1} \|\Delta \mathbf{p}_i\|^2 \right)^{\frac{1}{2}} \quad (2)$$

where  $\Delta \mathbf{p}_i$  is the error between the estimated position and reference trajectory position in a single state.

In the first tests conducted in a simulator as described by (Karjalainen et al. 2023), the VINS-Fusion estimate was found to be more accurate when the  $t_d$  value was fixed to constant, compared to when the online estimation method (Qin and Shen 2018) was used. For this reason, during the test flights, the  $t_d$  value was fixed to the one obtained from kalibr. However, the calibration estimate is never perfect and the prototype did not have actual hardware synchronization between the camera and the autopilot IMU. For that reason, after the test flights, the VINS-Fusion estimation was also run with online estimated  $t_d$  with the camera and IMU data recorded during the flight tests. The estimates were performed with the drone’s onboard computer, and the  $t_d$  estimate obtained with kalibr was used as the initial value of online estimation.

Since the coded targets are easily detectable, unique, and unnatural objects, the loop detection capability of VINS-Fusion was evaluated in a natural forest environment in Paloheinä, without the use of artificial targets. Since there were no coded targets for forming the reference trajectories, only the ability to detect the loops inside dense natural forest was tested, and the accuracy of the loop corrected trajectory was not evaluated. VINS-Fusion estimate with the loop detection algorithm was ran for the collected data with the drone’s onboard computer, and the effect of amount of features in pictures for loop detection capability was examined.

### 3.7.2. DBH estimation performance

The accuracy of the DBH estimation from the drone point cloud data was evaluated using Terrestrial Laser Scanning (TLS) data as a reference. The TLS scanings were conducted in April 2020, and tree height, diameter at breast height (DBH), and other parameters were estimated from the dataset. The estimated accuracy of the DBH mea-

surement was less than 1 cm.

Several metrics were used to evaluate the accuracy of the DBH estimation, including Root Mean Square Error (RMSE), Relative RMSE (RMSE%), Bias, Relative Bias (bias%), and Standard Deviation.

The RMSE measures the square root of the average of the squared differences between the estimated and reference DBH values. Bias indicates the average deviation between the estimated and reference DBH values.

$$\text{RMSE} = \sqrt{\frac{1}{n} \sum_{i=1}^n (d_{\text{estimated},i} - d_{\text{reference},i})^2} \quad (3)$$

where  $n$  is the total number of observations,  $d_{\text{estimated},i}$  is the estimated DBH, and  $d_{\text{reference},i}$  is the reference DBH.

$$\text{Bias} = \frac{1}{n} \sum_{i=1}^n (d_{\text{estimated},i} - d_{\text{reference},i}) \quad (4)$$

Relative RMSE (RMSE%) is computed by dividing the RMSE by the mean of the reference DBH values and multiplying by 100 to express it as a percentage. Relative Bias (Bias%) is determined by dividing the Bias by the mean of the reference DBH values and multiplying by 100.

$$\text{Relative RMSE (\%)} = \frac{\sqrt{\frac{1}{n} \sum_{i=1}^n (d_{\text{estimated},i} - d_{\text{reference},i})^2}}{\bar{d}_{\text{reference}}} \times 100 \quad (5)$$

$$\text{Relative Bias (\%)} = \frac{\frac{1}{n} \sum_{i=1}^n (d_{\text{estimated},i} - d_{\text{reference},i})}{\bar{d}_{\text{reference}}} \times 100 \quad (6)$$

Additionally standard deviation was calculated with following equation:

$$\text{SD} = \sqrt{\frac{1}{n} \sum_{i=1}^n (d_{\text{estimated},i} - \bar{d}_{\text{reference}})^2} \quad (7)$$

where  $\bar{d}_{\text{reference}}$  is the mean of the reference DBH values, and SD is the standard deviation.

Additionally, the completeness of stem detection was evaluated by comparing the total number of reference trees found from the drone-collected point cloud data to the total number of reference trees within the point cloud boundary.

$$c = \frac{r}{t} \times 100 \quad (8)$$

where  $c$  represents completeness (%),  $r$  is the number of reference trees found, and  $t$  is the total number of reference trees.

The impact of tree growth between the collection of drone data and reference measurements was not taken into account. Variability in tree growth, influenced by factors such as species, locations, health, age, is acknowledged as a source of error. Considering that the tree growth was relatively constant in the test area, forming a major component of the bias in the estimates. Additionally, some reference trees fell between the measurements and were not included in the estimations.

## 4. Results

### 4.1. *Autonomous navigation performance*

#### 4.1.1. *Obstacle avoidance*

The task of avoiding collisions during the flight is naturally more demanding in a dense forest than in a sparse forest. Consistent with these expectations, the trajectories were smoother and the success rate was better in "Evo-medium" than in "Evo-difficult" test area. In "Evo-medium" all performed test flights were successful and five out of seven test flights were performed with smooth trajectories. In "Evo-difficult" one of nine test flights failed and none of the test flights was performed with a smooth trajectory.

The reason for emergency stops in both environments was late detection of thin and dry spruce branches. In the failed test flight in "Evo-difficult" the reason was also a collision to a similar thin low branch.

The test flight success rates in both test forests are summarized in the Table 3. Figure 6 presents examples of performed trajectories and obtained point clouds in all test forests.

Table 3.: Test flight success in the test forests

Test areas	Forest type	Density (trees/ha)	Flight lengths (m)	Successful flights	Smooth trajectories
"Evo-medium"	Old Spruce forest	650	34 - 36	7/7	5/7
"Evo-difficult"	Young Spruce forest	2000	42	8/9	0/8

#### 4.1.2. *VIO*

The trajectory estimate error against the reference trajectory was successfully calculated for five flights in the medium forest and for three flights in the difficult forest. In the difficult forest, one of the flights was performed without coded targets making the reference trajectory non-comparable to others, in one flight there was a gap in the recorded onboard data due to a data recording error during a flight, and in one flight Metashape failed to retrieve the reference path. Average  $ATE_{pos}$  was 0.50 m in the medium forest and 0.34 m in the difficult forest. The standard deviation between  $ATE_{pos}$  was 0.06 m in the medium forest and 0.07 m in the difficult forest.

The VINS-Fusion estimates with online  $t_d$  estimation were calculated afterwards for the same flights. With online  $t_d$  estimation, average  $ATE_{pos}$  was 0.47 m in the medium forest and 0.33 m in the difficult forest. The standard deviation between  $ATE_{pos}$  was 0.02 m in the medium forest and 0.04 m in the difficult forest.

As the small standard deviation between the  $ATE_{pos}$  estimates indicates, the error between the VINS-Fusion estimates and the reference trajectories was similar in all

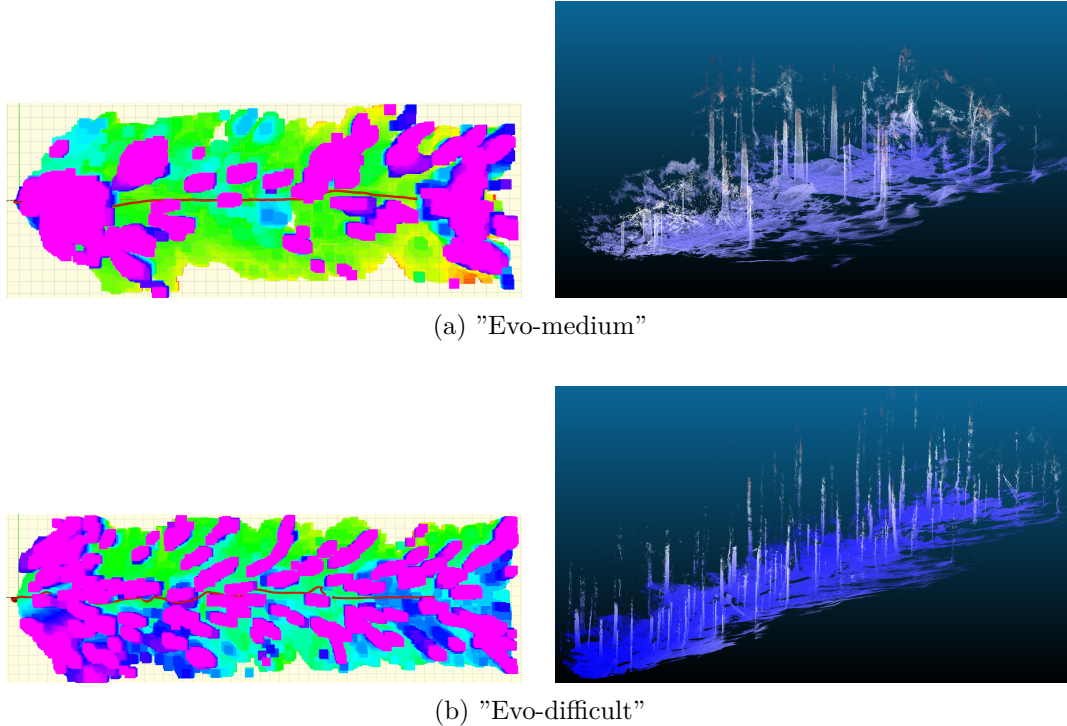


Figure 6.: Examples of drones own navigation grid maps with performed trajectories (left) and obtained point clouds (right) in (a) "Evo-medium" and (b) "Evo-difficult"

flights. In every flight, VINS-Fusion was estimating the shape of the trajectory well but underestimating the flight distance. Figure 7 presents an example of VINS-Fusion trajectory estimate and the reference trajectory in the difficult test forest. Table 4 presents the VINS-Fusion estimate errors in all flights.

Table 4.: VINS-Fusion estimation Errors in all test flights

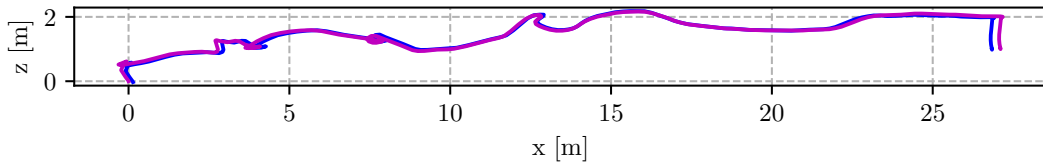
Test area	Flight No.	$ATE_{\text{pos}}$ (constant $t_d$ )	$ATE_{\text{pos}}$ (online estimated $t_d$ )
"Evo-medium"	1	0.5567	0.4816
"Evo-medium"	2	0.5599	0.4790
"Evo-medium"	3	0.4538	0.4769
"Evo-medium"	4	0.4945	0.4722
"Evo-medium"	5	0.4313	0.4400
"Evo-difficult"	1	0.3787	0.3340
"Evo-difficult"	2	0.3853	0.3727
"Evo-difficult"	3	0.2680	0.2962

Figure 8 shows an example of VINS-Fusion tracking image during a test flight in the dense test forest. The algorithm detects stable features to track from all parts of the picture. The image shows also flying dry leaves blown up by the air flow from the propellers of the drone. The moving leaves did not cause visible disturbances to the tracking of the pose.

In the loop closure tests, VINS-fusion detected a loop closure between 20 image pairs in the shorter path and four image pairs in the longer path with the same feature tracking parameters (Table 2) that were used in the flight tests. Figure 9 shows examples



(a) Top view



(b) Side view

Figure 7.: Example of a VINS-Fusion trajectory estimate and a reference trajectory obtained with Agisoft Metashape in the difficult forest from a) top and b) side.

of detected loop closure image pairs from both paths. The number of detected loops can be increased by increasing the amount of features per image in the VINS-Fusion configuration. By reducing the minimum distance between features from 40 to 35 pixels, VINS-Fusion detected a loop closure between 52 image pairs in the shorter path and 23 image pairs in the longer path. By decreasing the minimum distance between features to 30 pixels, VINS-Fusion detected a loop closure between 82 image pairs in the shorter path and 63 image pairs in the longer path. However, increasing the number of features also increases the computational burden of the VIO, and the effects on the real-time performance during flying were not tested in this study.

## 4.2. Forest reconstruction and analysis

### 4.2.1. Photogrammetric processing

Results of the photogrammetric processing are given in Table 5. In the image alignment process, all images were aligned in each dataset, which indicated successful processing. Re-projection errors varied between 0.29 and 0.39 pixels. The estimated flight GSDs (Ground Sampling Distance) ranged between 4.08 and 6.17 mm at ground level. Dis-



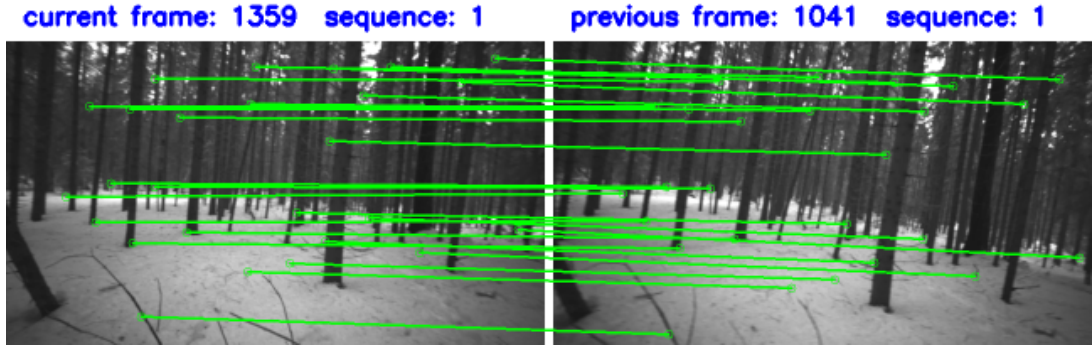
Figure 8.: Example of VINS-Fusion tracking image visualizing the tracked features. The tracking was not disturbed by the dry leaves blown by the air flow from the propellers of the drone. The coloring of the feature markers depends on the time how long the feature has been tracked. Blue dots symbolize new features and red features have been tracked longer.

tances from the trees varied between 0.55 and 7.94 m, resulting in GSDs of 0.85 - 12.34 mm at the objects of interest. Point clouds from datasets II-IV had similar point densities of 2.63-2.84 points/cm<sup>2</sup>, while dataset I provided a slightly higher point density of 3.58 points/cm<sup>2</sup>.

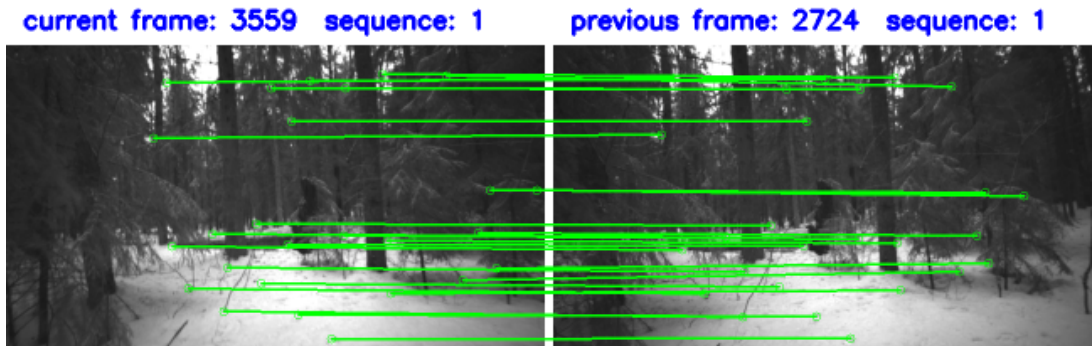
Results of accuracy estimation using Check Points (CPs) are shown in Table 6. The cases without GCPs or with one GCP at the beginning of the trajectory provided similar 2D and 3D RMSEs, of 11.36-11.72 cm and 11.37-11.73 cm, respectively. When two GCPs were used, the 2D and 3D RMSE improved to 5.26 cm and 5.48 cm, respectively. Adding an additional GCP resulted in a significant improvement in the 2D and 3D RMSE, reducing them to 1.41 cm and 1.48 cm, respectively.

#### 4.2.2. Tree detection

Figure 11 shows post-processed trajectories for dataset I-IV, as well as reference and detected trees, and the boundaries of the point clouds. I and II followed almost the same trajectory, while III and IV had similar trajectories. Dataset I trajectory was smoothest and it did not include any sharp turns. Other 3 trajectories had one or more sharper turns. For datasets I, II, III and IV, the total number of reference trees inside the point cloud boundary was 29, 29, 31 and 32, of which 23, 18, 19 and 20 were found from drone-collected point cloud. The resulting completeness values were 79.31%, 62.07%, 61.29% and 62.5%, respectively. The total number of different trees found was 29 out of 33 (87.88%) from dataset I-IV. However, when all the flights were processed simultaneously (combined) that resulted only 33.33 % completeness, where only 12 of 36 trees was found. When utilizing 0, 1, 2 and 3 gcps in dataset I completeness values were 72.41 %, 68.97 %, 75.86 % and 79.31 %, respectively (Table 5).



(a) Shorter path.



(b) Longer path.

Figure 9.: Example of image pairs where VINS-Fusion detects a scene to already visited one and performs a loop closure.

Table 5.: Photogrammetric processing results. Img. count: Number images/Number of aligned images; Number of GCPs; Completeness % (Number of trees found/Number of total trees); Reprojection error (pix); Number of tie points (in millions); Point density (points/cm<sup>2</sup>) in "Evo-medium" test site. I: Trajectory 1, II: Trajectory 2, III: Trajectory 3, IV: Trajectory 4, Combined: Trajectories 1-4 merged, and for Trajectory 1  $I_{0GCP}$ : no GCPs,  $I_{1GCP}$ : 1 GCP,  $I_{2GCP}$ : 2 GCPs,  $I_{3GCP}$ : 3 GCPs

Dataset	Img. count	N GCPs	Completeness (%)	Reproj. error (pix)	Num. tie points (millions)	Point density (points/cm <sup>2</sup> )
I	650/650	15	79.31 (23/29)	0.39	197132	3.58
II	648/648	15	62.07 (18/29)	0.33	151889	2.84
III	619/619	11	61.29 (19/31)	0.33	151083	2.63
IV	597/597	15	62.50 (20/32)	0.33	141716	2.66
Combined	2514/2514	15	33.33 (12/36)	0.29	1547828	8.53
$I_{0GCP}$	650/650	0	72.41 (21/29)	0.39	197132	3.54
$I_{1GCP}$	650/650	1	68.97 (20/29)	0.39	197132	3.54
$I_{2GCP}$	650/650	2	75.86 (22/29)	0.39	197132	3.54
$I_{3GCP}$	650/650	3	79.31 (23/29)	0.39	197132	3.54

In dataset I, the stem detection algorithm failed to detect one large tree and two small trees located near the drone's trajectory, despite these trees being well-reconstructed in the point cloud. Similarly, number of well-reconstructed trees but not detected by algorithm was 4, 5 and 5, in dataset II, III and IV, respectively. The three extra trees that were not identified in dataset I, were situated further from the trajectory and

Table 6.: Accuracy estimation (Root Mean Square Error; RMSE) using Check Points (CPs) and Camera Location in "Evo-medium" test site, for trajectory 1:  $I_{0GCP}$ : no GCPs,  $I_{1GCP}$ : 1 GCP,  $I_{2GCP}$ : 2 GCPs,  $I_{3GCP}$ : 3 GCPs

Dataset	Check Points (CPs) RMSE (cm)						Camera location RMSE (cm)				
	N CPs	X	Y	Z	2D	3D	$X_0$	$Y_0$	$Z_0$	2D <sub>0</sub>	3D <sub>0</sub>
$I_{0GCP}$	15	6.99	8.95	0.65	11.36	11.37	7.06	9.07	0.30	11.49	11.50
$I_{1GCP}$	14	7.19	9.25	0.56	11.72	11.73	7.03	9.06	0.28	11.47	11.47
$I_{2GCP}$	13	5.01	1.61	1.52	5.26	5.48	7.03	9.06	0.28	11.47	11.47
$I_{3GCP}$	12	1.19	0.75	0.45	1.41	1.48	1.46	0.70	0.56	1.62	1.71

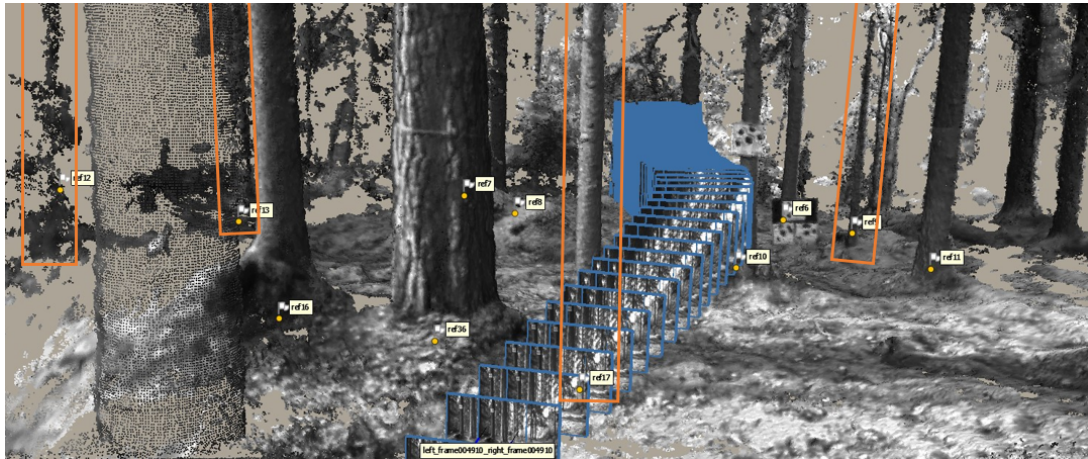


Figure 10.: GCPs, stereo images and reference trees visualized during the point cloud processing in the Agisoft Metashape (Metashape Development Team, 2021). Detected reference trees are marked, while those not detected are highlighted with a orange box.

exhibited poor reconstruction quality in the point cloud. The datasets II through IV each contained 7 poorly reconstructed trees. Many of these trees were located at a greater distance from the trajectory, while others were obscured from the camera's view by intervening trees.

#### 4.2.3. DBH estimation

RMSE and bias of the DBH estimates of datasets I-IV were similar, ranging from 3.33 to 3.86 cm (10.69-12.98%) and -0.67 to 1.40 (-2.11-4.71%), respectively (Table 7). Processing all the flights simultaneously (Combined) provided only marginally better results with an RMSE of 2.91 cm (9.14%) and a bias of 1.51 cm (4.74%).

When considering the impact of the number of GCPs, the utilization of 3, 2, 1 and 0 GCPs in photogrammetric processing yielded slightly poorer results compared to those obtained with all GCPs. The RMSE and bias values ranged from 3.93 to 4.37 cm (13.68%-14.66%) and 1.12 to 2.13 cm (3.89-7.55%), respectively (Table 7).

Tree size had an impact on the DBH estimation accuracy (Table 7). For small and medium-sized trees, with a DBH smaller than 30 cm, DBH estimations achieved superior performance in all dataset, with RMSE and bias varying from 1.16 to 2.75 cm (5.74-12.47%) and -0.01 to 0.62 cm (-0.06-3.14%), respectively. Significantly poorer per-

formance was obtained for trees with a DBH greater than 30 cm, with RMSE and bias ranging from 4.04 to 11.08 cm (8.99-25.44%) and -0.66 to 2.08 cm (-1.53-5.65%), respectively. This is demonstrated in Figure 13, illustrating a positive correlation between tree diameter and DBH estimation error. Notably, when the tree diameter exceeded 30 cm, the DBH estimation errors became more pronounced.

Analysis of the impact of the camera distance from trees did not reveal significant correlation between tree distance and DBH estimation errors (Figure 12).

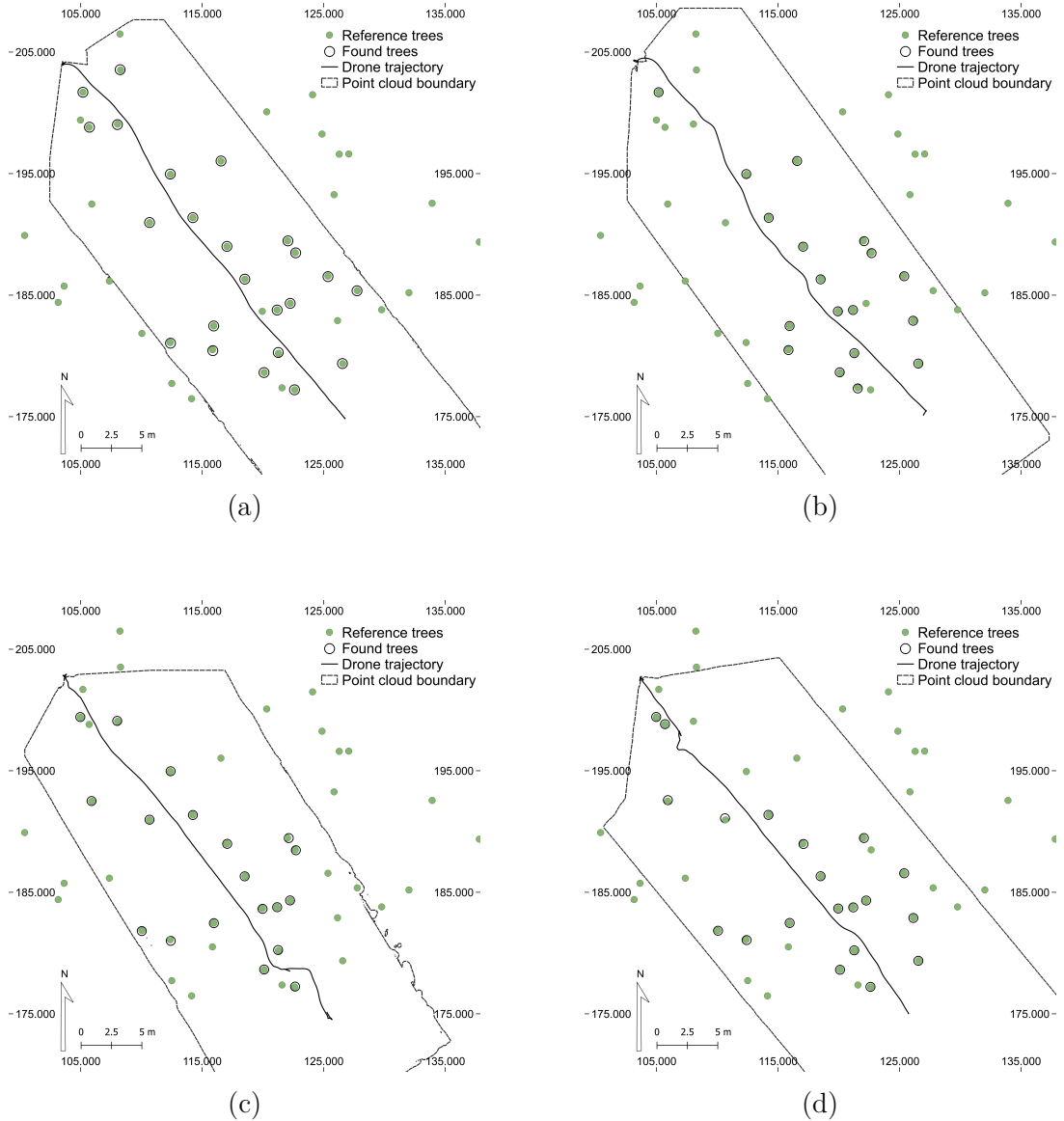


Figure 11.: Post-processed trajectories, reference trees and found trees in Dataset (a) I (b) II (c) III (d) IV..

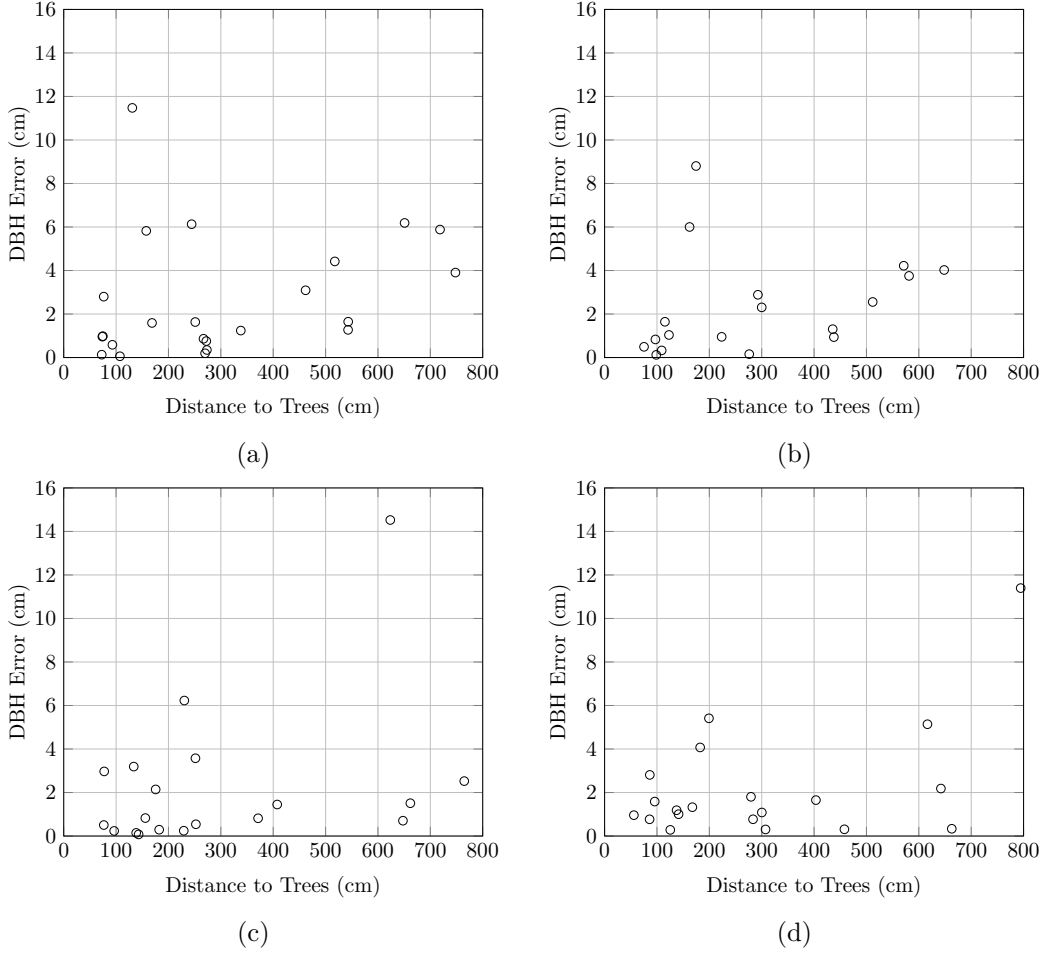


Figure 12.: Scatter plots of DBH errors with respect to distance to trees. Dataset (a) I (b) II (c) III (d) IV.

## 5. Discussion and Conclusions

### 5.1. *Autonomous flying*

The performance of autonomous navigation was promising in both test forests. The obstacle avoidance success rate was 100% in the medium forest and 87.5% in the difficult forest. However, the smoothness of the trajectories suffered from the increasing forest density. While in the medium forest, 71.4% of the flights had a smooth trajectory, in the difficult forest at least one emergency stop was needed in all of the flights. Further consideration should be given to finding the optimal sensor for detecting thin and dry branches earlier. Nonetheless, the current prototype already allows reliable and safe autonomous obstacle avoidance in easy and medium difficulty level boreal forests.

The accuracy of the position estimate by VINS-Fusion was satisfying for short flights performed in this study, but in the longer flights, the error would start to accumulate making the position errors high. However, the standard deviation between the errors between the test flights was small, and the VINS-Fusion systematically estimated the flight paths shorter than in reality (as can be seen from Figure 7). This suggests, that a notable part of the position error could be eliminated by improving the calibration

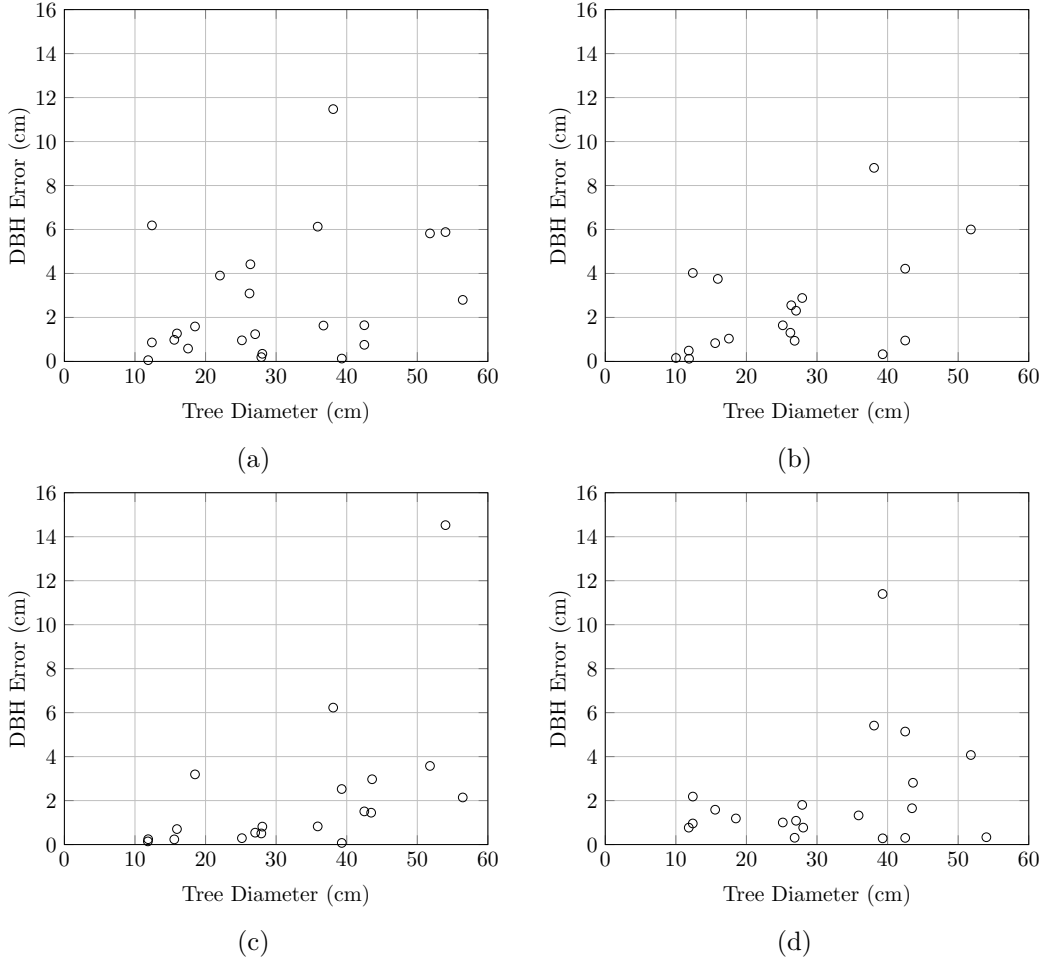


Figure 13.: Scatter plots of DBH errors with respect to diameter of trees. Dataset (a) I (b) II (c) III (d) IV

of the sensor setup. The results suggest that the estimates by VINS-Fusion were more accurate with online  $t_d$  estimation than when the  $t_d$  value was fixed to the one obtained from the calibration. However, further development of the prototype should include implementing hardware-level synchronization between the camera and the IMU of the autopilot.

The position error can also be reduced by optimizing the estimate with loop closures, and the results from the walking tests showed that VINS-Fusion could detect loop closures even in a homogeneous forest environment. Increasing the number of features tracked by VINS-Fusion increases the number of detected loops. However, increasing the number of features increases also the computational burden of the system potentially disrupting the real-time estimation. Finding the optimal value for the tracked features as well as measuring the actual improvement of the loop closures to the position estimate requires further studies.

Table 7.: Accuracy of the stem diameter breast height (DBH) in "Evo-medium" test site. Dataset is split in 3 categories: All, DBH < 30 cm and DBH > 30 cm trees. Datasets: I: Flight 1, II: Flight 2, III: Flight 3, IV: Flight 4, Combined: Flights I-IV merged, and for Dataset I:  $I_{0GCP}$ : with no GCPs,  $I_{1GCP}$ : with 1 GCP,  $I_{2GCP}$ : with 2 GCPs,  $I_{3GCP}$  with 3 GCPs.

Dataset	Number of trees	RMSE (cm)	RMSE%	Bias (cm)	Bias%	Standard Deviation
	All <30 cm >30 cm					
I	23	3.86	12.98	1.40	4.71	3.60
	14	2.56	12.47	0.17	0.85	2.54
II	9	5.29	11.98	1.23	2.78	4.26
	17	3.33	12.79	1.01	3.87	3.17
	12	2.16	11.36	0.31	1.63	2.12
III	5	5.14	12.01	0.70	1.63	4.56
	19	3.97	12.05	0.97	2.95	3.85
	9	1.16	5.74	0.13	0.64	1.13
IV	10	5.36	12.07	0.84	1.89	5.12
	20	3.40	10.69	-0.67	-2.11	3.33
	10	1.28	6.21	-0.01	-0.06	1.28
Combined	10	4.63	10.77	-0.66	-1.53	4.44
	12	2.91	9.14	1.51	4.74	2.49
	7	1.41	6.70	-0.12	-0.56	1.39
$I_{0GCP}$	6	4.04	8.99	1.63	3.62	1.87
	21	4.37	14.66	1.61	5.42	4.06
	12	2.75	13.07	-0.20	-0.97	2.73
$I_{1GCP}$	9	7.93	18.62	2.41	5.65	5.17
	20	4.38	14.71	1.68	5.65	4.04
	12	2.02	9.63	-0.01	-0.06	2.02
$I_{2GCP}$	8	6.46	15.06	1.69	3.95	4.88
	23	4.35	15.43	2.13	7.55	3.79
	14	1.77	8.98	0.62	3.14	1.48
$I_{3GCP}$	8	11.08	25.44	2.08	4.77	8.96
	23	3.93	13.68	1.12	3.89	3.77
	14	1.22	6.23	0.14	0.72	1.20
	9	6.10	14.20	0.98	2.27	5.57

## 5.2. Accuracy of forest measurements

The proposed system was assessed by comparing it to other relevant studies (Section 2.2, Table 1) considering the accuracy, system autonomy and weight, and complexity of test environment.

The highest accuracy UAV SfM-MVS results were presented by Shimabuku, Konoshima, and Ota (2023) with an RMSE of 0.4 cm (3.2%). However, their test site included only 7 reference trees. Kuželka and Surový (2018) and Krisanski, Taskhiri, and Turner (2020) had more reference trees and achieved similar DBH accuracy compared to that in this study, but the flights were piloted manually. Notably, the SfM-MVS approaches involved light-weight systems.

The fully automated under-canopy UAV Lidar system (ULS) by Liang et al. (2024) weighted 5 kg and provided an RMSE of 4.48 cm (21.37%) and bias of 5.01 (14.91%) at best. Wang et al. (2021) combined data from above- and under-canopy drone with a Riegl miniVUX-1 UAV lidar (Riegl GmbH, Horn, Austria), resulting in an RMSE of 7.95 cm (33.35%) and bias of 3.72 cm (15.61%). Their under-canopy flight was carried out manually by a pilot and the system weighted approximately 10 kg. Muhojoki et al. (2024) carried out manually flown flights in three sparse density forest plots with the Deep

Forest drone utilized an Ouster OS0-32 Rev. 5 laser scanner (Ouster, San Francisco, CA, USA) and the Hovermap drone equipped with a Velodyne VLP-16 laser scanner (Velodyne Lidar, San Jose, CA, USA), resulting in an averaged RMSE of 1.5 cm (6.7 %) and 1.6 cm (6.9 %) and bias of -0.7 cm (3.0 %) and -0.1 cm (-0.6 %). However, without utilizing their bias removal method RMSE and bias were significantly higher. The highest accuracy DBH estimates with under-canopy LiDAR were presented by Hyyppä et al. (2020a) resulting in an RMSE of 0.6 cm (2.3%) and bias of 0.34 cm (1.3%) in a sparse forest and 1.1 cm (3.5%) and 0.12 cm (0.4%) in a medium density forest. Their system was also manually piloted and weighted approximately 10 kg, a Tarot 960 UAV equipped with Kaarta Stencil-1 (VLP-16) LiDAR (Kaarta, Pittsburgh, Pennsylvania, USA).

Summarizing, the highest accuracy levels were obtained with the relatively heavy ULS systems, which were operated manually in sparse forest environments. Miniaturized lightweight sensors were used in the studies by Shimabuku, Konoshima, and Ota (2023), Krisanski, Taskhiri, and Turner (2020), and Kuželka and Surovỳ (2018), and Liang et al. (2024). Results from the SfM-MVS systems were comparable to each other but ULS provided slightly poorer accuracy. Only studies by Shimabuku, Konoshima, and Ota (2023) and Liang et al. (2024) had flights with a high level of automation. Considering the complexity of the environments, the forest by Liang et al. (2024) (1000 trees/ha) was the closest to that in this study (650 and 2000 trees/ha), while other studies were conducted in remarkably sparser forests.

Based on the previous, it can be concluded that when considering the combination of accuracy, autonomy of flying, and environmental complexity, the proposed system introduced a new level of performance for under-canopy forest reconstruction. The results show the great promise of miniaturized camera SfM-MVS in autonomous under-canopy forest reconstruction.

### 5.3. *Potential improvements and future work*

During the evaluation of the system, some areas for improvement were identified, which can help develop the method towards a tool in practical forest measurements.

The reliability of the navigation could be improved by performing further research on potential sensors and methods for detecting the thin branches. Blindsides in the mapping could be tackled either by sensors with 360° FOV (e.g. Lidar, 360° camera or multi-camera system) or storing historical data to occupancy grid maps in addition to the currently visible area.

The virtual floor and ceiling of Ego-planner-V2 (Zhou et al. 2022) are also defined as static with respect to the initial altitude of the drone limiting the low-altitude flying to relatively flat areas. To comprehensively map uneven forest plots, the altitude limits should be modified to be dynamic and with respect to the local terrain level.

The drift compensation is one of the important future development goals. Loop closure tests provided promising results and potential future tests could evaluate the approach by performing block flights. In addition to the loop closures, the error in the position estimate could potentially be further reduced by fusing GNSS data to the VIO estimate. The potential methods for GNSS-Fusion include using the global fusion features in VINS-Fusion (Qin et al. 2019a) or replacing VINS-Fusion with another method fusing GNSS-data and VIO, e.g. GVINS (Cao, Lu, and Shen 2022). Even though the dense forest canopy blocks the GNSS signals, during long-term operations the drone could receive corrections to the position estimate in the open areas while relying on the

VIO estimate in denser parts of the forests.

It is also notable that the rigorous photogrammetric post-processing effectively compensated for the systematic errors. While the real-time trajectory error was 50 cm, the post-processed 3D error was approximately 11 cm without any GCPs, this correlates with the trajectory error. Therefore, for applications relying on post-processing, drift is not expected to pose significant issues, especially when covering small areas such as forest test plots.

In this study, the performed flight paths were straight flights through the sample plots, and the DBH estimation was performed only for the tree trunks recorded during that path. For more comprehensive forest characterization, the trajectory should cover the whole test plot, and observe the trees from multiple sides. The global path covering the whole test plot could be implemented either with a simple waypoint generation algorithm as Liang et al. (2024) or with more advanced exploration methods such as proposed by Zhou et al. (2021a) or Cieslewski, Kaufmann, and Scaramuzza (2017). Another way to achieve area coverage would be utilizing a swarm of drones as in the original article by Zhou et al. (2022). Furthermore, recent exploration algorithms (Zhou, Xu, and Shen 2023)(Bartolomei, Teixeira, and Chli 2023) are able to utilize drone swarms to further improve and speed up the area coverage.

While this study only demonstrated the potential of forest characteristics estimation through DBH estimation and tree detection, the scope of data collection is not limited to that. Having a second camera pointing upwards would enable a more comprehensive reconstruction of the tree trunks to perform also stem curve estimation based on the point clouds. With a developed camera-based prototype, the data collection is not limited to point clouds, but also applications of image based mapping and object detection can be developed on top of it. Potential applications could include e.g. classifying and counting species of trees and other vegetation as well as monitoring damages in the bark of the trees due to insect pests.

The prototype opens also possibilities for research of real-time forest characteristics analysis. In this study, the point clouds were obtained with post-processing, but the utilized onboard camera Intel Realsense D435 can also produce 3D point clouds in real-time. Image-based object detection can also be performed in real-time e.g. with YOLO. The analysis can be performed either with the onboard computer or with a remote computer or cloud service over the Internet connection.

## 6. Acknowledgements

This research was funded by the Research Council of Finland within projects “Learning techniques for autonomous drone based hyperspectral analysis of forest vegetation” (decision no. 357380), Fireman (decision no. 346710), and the Research Council of Finland Flagship Forest–Human–Machine Interplay—Building Resilience, Redefining Value Networks and Enabling Meaningful Experiences (UNITE) (decision no. 357908).

## References

Ahmad, Afzal, Daniel Bonilla Licea, Giuseppe Silano, Tomas Baca, and Martin Saska. 2022. “PACNav: A collective navigation approach for UAV swarms deprived of communication and external localization.” *Bioinspiration & Biomimetics* <https://doi.org/10.1088/1748-3190/ac98e6>.

- Balenović, Ivan, Xinlian Liang, Luka Jurjević, Juha Hyyppä, Ante Seletković, and Antero Kukko. 2021. “Hand-held personal laser scanning—current status and perspectives for forest inventory application.” *Croatian Journal of Forest Engineering: Journal for Theory and Application of Forestry Engineering* 42 (1): 165–183.
- Bartolomei, Luca, Lucas Teixeira, and Margarita Chli. 2023. “Fast Multi-UAV Decentralized Exploration of Forests.” *IEEE Robotics and Automation Letters* 8 (9): 5576–5583. <https://doi.org/10.1109/LRA.2023.3296037>.
- Bauwens, Sébastien, Harm Bartholomeus, Kim Calders, and Philippe Lejeune. 2016. “Forest inventory with terrestrial LiDAR: A comparison of static and hand-held mobile laser scanning.” *Forests* 7 (6): 127.
- Bienert, A, S Scheller, E Keane, F Mohan, and C Nugent. 2007. “Tree detection and diameter estimations by analysis of forest terrestrial laserscanner point clouds.” In *ISPRS workshop on laser scanning*, Vol. 36, 50–55. Citeseer.
- Bienert, Anne, Louis Georgi, Matthias Kunz, Hans-Gerd Maas, and Goddert Von Oheimb. 2018. “Comparison and combination of mobile and terrestrial laser scanning for natural forest inventories.” *Forests* 9 (7): 395.
- Brede, Benjamin, Alvaro Lau, Harm M Bartholomeus, and Lammert Kooistra. 2017. “Comparing RIEGL RiCOPTER UAV LiDAR derived canopy height and DBH with terrestrial LiDAR.” *Sensors* 17 (10): 2371.
- Cabo, Carlos, Susana Del Pozo, Pablo Rodríguez-González, Celestino Ordóñez, and Diego González-Aguilera. 2018. “Comparing terrestrial laser scanning (TLS) and wearable laser scanning (WLS) for individual tree modeling at plot level.” *Remote Sensing* 10 (4): 540.
- Calonder, Michael, Vincent Lepetit, Christoph Strecha, and Pascal Fua. 2010. “BRIEF: Binary Robust Independent Elementary Features.” In *Computer Vision – ECCV 2010*, edited by Kostas Daniilidis, Petros Maragos, and Nikos Paragios, Berlin, Heidelberg, 778–792. Springer Berlin Heidelberg.
- Campos-Macías, Leobardo, Rodrigo Aldana-López, Rafael de la Guardia, José I Parra-Vilchis, and David Gómez-Gutiérrez. 2021. “Autonomous navigation of MAVs in unknown cluttered environments.” *Journal of Field Robotics* 38 (2): 307–326. <https://doi.org/doi.org/10.1002/rob.21959>.
- Cao, Shaozu, Xiuyuan Lu, and Shaojie Shen. 2022. “GVINS: Tightly Coupled GNSS–Visual–Inertial Fusion for Smooth and Consistent State Estimation.” *IEEE Transactions on Robotics* 38 (4): 2004–2021. <https://doi.org/10.1109/TRO.2021.3133730>.
- Chen, Shilin, Haiyang Liu, Zhongke Feng, Chaoyong Shen, and Panpan Chen. 2019. “Applicability of personal laser scanning in forestry inventory.” *PLoS One* 14 (2): e0211392.
- Chisholm, Ryan A, Jinqiang Cui, Shawn KY Lum, and Ben M Chen. 2013. “UAV LiDAR for below-canopy forest surveys.” *Journal of Unmanned Vehicle Systems* 1 (01): 61–68.
- Cieslewski, Titus, Elia Kaufmann, and Davide Scaramuzza. 2017. “Rapid exploration with multi-rotors: A frontier selection method for high speed flight.” In *2017 IEEE/RSJ International Conference on Intelligent Robots and Systems (IROS)*, 2135–2142.
- Ester, Martin, Hans-Peter Kriegel, Jörg Sander, and Xiaowei Xu. 1996. “A density-based algorithm for discovering clusters in large spatial databases with noise.” In *Kdd*, Vol. 96, 226–231.
- ETH Zürich Autonomous Systems Lab. 2023. “kalibr - IMU Noise Model.” ETH Zürich. <https://github.com/ethz-asl/kalibr/wiki/IMU-Noise-Model>. Accessed: 2024-05-27.
- Feng, Baokun, Sheng Nie, Cheng Wang, Xiaohuan Xi, Jinliang Wang, Guoqing Zhou, and Haoyu Wang. 2022. “Exploring the potential of UAV LiDAR data for trunk point extraction and direct DBH measurement.” *Remote Sensing* 14 (12): 2753.
- Forsman, Mona, Johan Holmgren, and Kenneth Olofsson. 2016. “Tree stem diameter estimation from mobile laser scanning using line-wise intensity-based clustering.” *Forests* 7 (9): 206.
- Furgale, Paul, Timothy D. Barfoot, and Gabe Sibley. 2012. “Continuous-time batch estimation using temporal basis functions.” In *2012 IEEE International Conference on Robotics and Automation*, 2088–2095.

- Furgale, Paul, Joern Rehder, and Roland Siegwart. 2013. “Unified temporal and spatial calibration for multi-sensor systems.” In *2013 IEEE/RSJ International Conference on Intelligent Robots and Systems*, 1280–1286.
- Galvez-López, Dorian, and Juan D. Tardos. 2012. “Bags of Binary Words for Fast Place Recognition in Image Sequences.” *IEEE Transactions on Robotics* 28 (5): 1188–1197. <https://doi.org/10.1109/TRO.2012.2197158>.
- Hyypä, Eric, Juha Hyypä, Teemu Hakala, Antero Kukko, Michael A Wulder, Joanne C White, Jiri Pyörälä, et al. 2020a. “Under-canopy UAV laser scanning for accurate forest field measurements.” *ISPRS Journal of Photogrammetry and Remote Sensing* 164: 41–60.
- Hyypä, Eric, Antero Kukko, Harri Kaartinen, Xiaowei Yu, Jesse Muhojoki, Teemu Hakala, and Juha Hyypä. 2022. “Direct and automatic measurements of stem curve and volume using a high-resolution airborne laser scanning system.” *Science of Remote Sensing* 5: 100050.
- Hyypä, Eric, Antero Kukko, Risto Kaijaluoto, Joanne C White, Michael A Wulder, Jiri Pyörälä, Xinlian Liang, et al. 2020b. “Accurate derivation of stem curve and volume using backpack mobile laser scanning.” *ISPRS Journal of Photogrammetry and Remote Sensing* 161: 246–262.
- Hyypä, Eric, Xiaowei Yu, Harri Kaartinen, Teemu Hakala, Antero Kukko, Mikko Vastaranta, and Juha Hyypä. 2020c. “Comparison of backpack, handheld, under-canopy UAV, and above-canopy UAV laser scanning for field reference data collection in boreal forests.” *Remote Sensing* 12 (20): 3327.
- Hyypä, Juha, Xiaowei Yu, Teemu Hakala, Harri Kaartinen, Antero Kukko, Heikki Hyyti, Jesse Muhojoki, and Eric Hyypä. 2021. “Under-canopy UAV laser scanning providing canopy height and stem volume accurately.” *Forests* 12 (7): 856.
- Intel Realsense Development Team. 2023. “Depth Camera D435.” Intel Corporation. <https://www.intelrealsense.com/depth-camera-d435/>.
- Karjalainen, V., T. Hakala, A. George, N. Koivumäki, J. Suomalainen, and E. Honkavaara. 2023. “A DRONE SYSTEM FOR AUTONOMOUS MAPPING FLIGHTS INSIDE A FOREST – A FEASIBILITY STUDY AND FIRST RESULTS.” *The International Archives of the Photogrammetry, Remote Sensing and Spatial Information Sciences XLVIII-1/W2-2023*: 597–603. <https://doi.org/10.5194/isprs-archives-XLVIII-1-W2-2023-597-2023>.
- Keselman, Leonid, John Iselin Woodfill, Anders Grunnet-Jepsen, and Achintya Bhowmik. 2017. “Intel(R) RealSense(TM) Stereoscopic Depth Cameras.” In *2017 IEEE Conference on Computer Vision and Pattern Recognition Workshops (CVPRW)*, 1267–1276.
- Kohlbrecher, Stefan, Oskar von Stryk, Johannes Meyer, and Uwe Klingauf. 2011. “A flexible and scalable SLAM system with full 3D motion estimation.” In *2011 IEEE International Symposium on Safety, Security, and Rescue Robotics*, 155–160.
- Krisanski, Sean, Mohammad Sadegh Taskhiri, and Paul Turner. 2020. “Enhancing Methods for Under-Canopy Unmanned Aircraft System Based Photogrammetry in Complex Forests for Tree Diameter Measurement.” *Remote Sensing* 12 (10). <https://doi.org/10.3390/rs12101652>, <https://www.mdpi.com/2072-4292/12/10/1652>.
- Kuan, Yau Weng, Ng Oon Ee, and Lee Sze Wei. 2019. “Comparative Study of Intel R200, Kinect v2, and Primesense RGB-D Sensors Performance Outdoors.” *IEEE Sensors Journal* 19 (19): 8741–8750. <https://doi.org/10.1109/JSEN.2019.2920976>.
- Kuželka, Karel, Martin Slavík, and Peter Surový. 2020. “Very high density point clouds from UAV laser scanning for automatic tree stem detection and direct diameter measurement.” *Remote Sensing* 12 (8): 1236.
- Kuželka, Karel, and Peter Surový. 2018. “Mapping forest structure using UAS inside flight capabilities.” *Sensors* 18 (7): 2245.
- Laasasenaho, Jouko. 1982. *Taper curve and volume functions for pine, spruce and birch*.
- Leica Geosystems. 2020. “Leica Nova TS60 Data sheet.” <https://leica-geosystems.com/products/total-stations/robotic-total-stations/leica-nova-ts60/>.
- Liang, Xinlian, Anttoni Jaakkola, Yunsheng Wang, Juha Hyypä, Eija Honkavaara, Jingbin Liu, and Harri Kaartinen. 2014a. “The use of a hand-held camera for individual tree 3D mapping in forest sample plots.” *Remote Sensing* 6 (7): 6587–6603.

- Liang, Xinlian, Antero Kukko, Juha Hyypä, Matti Lehtomäki, Jiri Pyörälä, Xiaowei Yu, Harri Kaartinen, Anttoni Jaakkola, and Yunsheng Wang. 2018. “In-situ measurements from mobile platforms: An emerging approach to address the old challenges associated with forest inventories.” *ISPRS Journal of Photogrammetry and Remote Sensing* 143: 97–107.
- Liang, Xinlian, Antero Kukko, Harri Kaartinen, Juha Hyypä, Xiaowei Yu, Anttoni Jaakkola, and Yunsheng Wang. 2014b. “Possibilities of a personal laser scanning system for forest mapping and ecosystem services.” *Sensors* 14 (1): 1228–1248.
- Liang, Xinlian, Yunsheng Wang, Jiri Pyörälä, Matti Lehtomäki, Xiaowei Yu, Harri Kaartinen, Antero Kukko, et al. 2019. “Forest in situ observations using unmanned aerial vehicle as an alternative of terrestrial measurements.” *Forest ecosystems* 6: 1–16.
- Liang, Xinlian, Haiyun Yao, Hanwen Qi, and Xiaochen Wang. 2024. “Forest in situ observations through a fully automated under-canopy unmanned aerial vehicle.” *Geo-spatial Information Science* 1–17.
- Liu, Wenyi, Yunfan Ren, and Fu Zhang. 2024. “Integrated Planning and Control for Quadrotor Navigation in Presence of Suddenly Appearing Objects and Disturbances.” *IEEE Robotics and Automation Letters* 9 (1): 899–906. <https://doi.org/10.1109/LRA.2023.3311358>.
- Liu, Xu, Guilherme V. Nardari, Fernando Cladera Ojeda, Yuezhan Tao, Alex Zhou, Thomas Donnelly, Chao Qu, et al. 2022. “Large-Scale Autonomous Flight With Real-Time Semantic SLAM Under Dense Forest Canopy.” *IEEE Robotics and Automation Letters* 7 (2): 5512–5519. <https://doi.org/10.1109/LRA.2022.3154047>.
- Loquercio, Antonio, Elia Kaufmann, René Ranftl, Matthias Müller, Vladlen Koltun, and Davide Scaramuzza. 2021. “Learning high-speed flight in the wild.” *Science Robotics* 6 (59): eabg5810. <https://doi.org/10.1126/scirobotics.abg5810>.
- Lucas, Bruce D, and Takeo Kanade. 1981. “An iterative image registration technique with an application to stereo vision.” In *IJCAI’81: 7th international joint conference on Artificial intelligence*, Vol. 2, 674–679.
- Marselis, Suzanne M, Marta Yebra, Tom Jovanovic, and Albert IJM van Dijk. 2016. “Deriving comprehensive forest structure information from mobile laser scanning observations using automated point cloud classification.” *Environmental modelling & software* 82: 142–151.
- Maye, Jérôme, Paul Furgale, and Roland Siegwart. 2013. “Self-supervised calibration for robotic systems.” In *2013 IEEE Intelligent Vehicles Symposium (IV)*, 473–480.
- Mellinger, Daniel, and Vijay Kumar. 2011. “Minimum snap trajectory generation and control for quadrotors.” In *2011 IEEE International Conference on Robotics and Automation*, 2520–2525.
- Metashape Development Team. 2021. “Agisoft Metashape Software, Version 1.7.” Agisoft LLC. <https://www.agisoft.com/downloads/installer/>.
- Mokroš, Martin, Jozef Východík, Julián Tomašík, Alžbeta Grznárová, Peter Valent, Martin Slavík, and Ján Merganič. 2018. “High precision individual tree diameter and perimeter estimation from close-range photogrammetry.” *Forests* 9 (11): 696.
- Moravec, Hans, and Alberto Elfes. 1985. “High resolution maps from wide angle sonar.” In *Proceedings. 1985 IEEE international conference on robotics and automation*, Vol. 2, 116–121. IEEE.
- Muhojoki, Jesse, Daniella Tavi, Eric Hyypä, Matti Lehtomäki, Tamás Faitli, Harri Kaartinen, Antero Kukko, Teemu Hakala, and Juha Hyypä. 2024. “Benchmarking Under- and Above-Canopy Laser Scanning Solutions for Deriving Stem Curve and Volume in Easy and Difficult Boreal Forest Conditions.” *Remote Sensing* 16 (10). <https://doi.org/10.3390/rs16101721>, <https://www.mdpi.com/2072-4292/16/10/1721>.
- Nguyen, Huan, Rasmus Andersen, Evangelos Boukas, and Kostas Alexis. 2023. “Uncertainty-aware visually-attentive navigation using deep neural networks.” *The International Journal of Robotics Research* 0 (0): 02783649231218720. <https://doi.org/10.1177/02783649231218720>.
- Olson, Edwin. 2011. “AprilTag: A robust and flexible visual fiducial system.” In *2011 IEEE International Conference on Robotics and Automation*, 3400–3407.
- Oxford Dynamic Robot Systems Group. 2022. “Allan Variance ROS.” University of Oxford.

- [https://github.com/ori-drs/allan\\_variance\\_ros](https://github.com/ori-drs/allan_variance_ros).
- Piermattei, Livia, Wilfried Karel, Di Wang, Martin Wieser, Martin Mokroš, Peter Surovỳ, Milan Koreň, Julián Tomašík, Norbert Pfeifer, and Markus Hollaus. 2019. “Terrestrial structure from motion photogrammetry for deriving forest inventory data.” *Remote Sensing* 11 (8): 950.
- Puliti, Stefano, Hans Ole Ørka, Terje Gobakken, and Erik Næsset. 2015. “Inventory of Small Forest Areas Using an Unmanned Aerial System.” *Remote Sensing* 7 (8): 9632–9654. <https://doi.org/10.3390/rs70809632>, <https://www.mdpi.com/2072-4292/7/8/9632>.
- PX4 Community. 2023. “PX4-Autopilot, Version 1.14.0.” <https://github.com/PX4/PX4-Autopilot>.
- Qin, Tong, Shaozu Cao, Jie Pan, and Shaojie Shen. 2019a. “A General Optimization-based Framework for Global Pose Estimation with Multiple Sensors.” *arXiv preprint arXiv:1901.03642* <https://doi.org/doi.org/10.48550/arXiv.1901.03642>.
- Qin, Tong, Peiliang Li, and Shaojie Shen. 2018. “Vins-mono: A robust and versatile monocular visual-inertial state estimator.” *IEEE Transactions on Robotics* 34 (4): 1004–1020. <https://doi.org/doi.org/10.1109/TRO.2018.2853729>.
- Qin, Tong, Jie Pan, Shaozu Cao, and Shaojie Shen. 2019b. “A general optimization-based framework for local odometry estimation with multiple sensors.” *arXiv preprint arXiv:1901.03638* <https://doi.org/doi.org/10.48550/arXiv.1901.03638>.
- Qin, Tong, and Shaojie Shen. 2018. “Online Temporal Calibration for Monocular Visual-Inertial Systems.” In *2018 IEEE/RSJ International Conference on Intelligent Robots and Systems (IROS)*, 3662–3669.
- Quigley, Morgan, Josh Faust, Tully Foote, Jeremy Leibs, et al. 2009. “ROS: an open-source Robot Operating System.” In *Proc. of the IEEE Intl. Conf. on Robotics and Automation (ICRA), Workshop on Open Source Robotics*, Kobe, Japan, May.
- Reddy Cenkeramaddi, Linga, Jyoti Bhatia, Ajit Jha, Santosh Kumar Vishkarma, and J. Soumya. 2020. “A Survey on Sensors for Autonomous Systems.” In *2020 15th IEEE Conference on Industrial Electronics and Applications (ICIEA)*, 1182–1187.
- Ren, Yunfan, Fangcheng Zhu, Wenyi Liu, Zhepei Wang, Yi Lin, Fei Gao, and Fu Zhang. 2022. “Bubble Planner: Planning High-speed Smooth Quadrotor Trajectories using Receding Corridors.” In *2022 IEEE/RSJ International Conference on Intelligent Robots and Systems (IROS)*, 6332–6339.
- Ryding, Joseph, Emily Williams, Martin J Smith, and Markus P Eichhorn. 2015. “Assessing handheld mobile laser scanners for forest surveys.” *Remote sensing* 7 (1): 1095–1111.
- Schubert, F. M., B. H. Fleury, P. Robertson, R. Prieto-Cerdeira, A. Steingass, and A. Lehner. 2010. “Modeling of multipath propagation components caused by trees and forests.” In *Proceedings of the Fourth European Conference on Antennas and Propagation*, 1–5.
- Shi, Jianbo, and Tomasi. 1994. “Good features to track.” In *1994 Proceedings of IEEE Conference on Computer Vision and Pattern Recognition*, 593–600.
- Shimabuku, Fu, Masashi Konoshima, and Ikuo Ota. 2023. “Diameter and stem volume estimation based on under canopy UAV-SfM-MVS survey approach in subtropical forest of Okinawa Island, Japan.” *FORMATH* 22: 22–004.
- Sturm, Jürgen, Nikolas Engelhard, Felix Endres, Wolfram Burgard, and Daniel Cremers. 2012. “A benchmark for the evaluation of RGB-D SLAM systems.” In *2012 IEEE/RSJ International Conference on Intelligent Robots and Systems*, 573–580.
- Surovỳ, Peter, Atsushi Yoshimoto, and Dimitrios Panagiotidis. 2016. “Accuracy of reconstruction of the tree stem surface using terrestrial close-range photogrammetry.” *Remote Sensing* 8 (2): 123.
- Umeyama, S. 1991. “Least-squares estimation of transformation parameters between two point patterns.” *IEEE Transactions on Pattern Analysis and Machine Intelligence* 13 (4): 376–380. <https://doi.org/10.1109/34.88573>.
- Usenko, Vladyslav, Lukas von Stumberg, Andrej Pangercic, and Daniel Cremers. 2017. “Real-time trajectory replanning for MAVs using uniform B-splines and a 3D circular buffer.” In *2017 IEEE/RSJ International Conference on Intelligent Robots and Systems (IROS)*,

- 215–222.
- Vandendaele, Bastien, Richard A Fournier, Udayalakshmi Vepakomma, Gaetan Pelletier, Philippe Lejeune, and Olivier Martin-Ducup. 2021. “Estimation of northern hardwood forest inventory attributes using UAV laser scanning (ULS): Transferability of laser scanning methods and comparison of automated approaches at the tree-and stand-level.” *Remote Sensing* 13 (14): 2796.
- Viljanen, Niko, Eija Honkavaara, Roope Näsi, Teemu Hakala, Oiva Niemeläinen, and Jere Kaivosoja. 2018. “A Novel Machine Learning Method for Estimating Biomass of Grass Swards Using a Photogrammetric Canopy Height Model, Images and Vegetation Indices Captured by a Drone.” *Agriculture* 8 (5): 70. <https://doi.org/10.3390/agriculture8050070>.
- Wallace, Luke, Arko Lucieer, Zbyněk Malenovský, Darren Turner, and Petr Vopěnka. 2016. “Assessment of forest structure using two UAV techniques: A comparison of airborne laser scanning and structure from motion (SfM) point clouds.” *Forests* 7 (3): 62.
- Wang, Yunsheng, Antero Kukko, Eric Hyyppä, Teemu Hakala, Jiri Pyörälä, Matti Lehtomäki, Aimad El Issaoui, et al. 2021. “Seamless integration of above-and under-canopy unmanned aerial vehicle laser scanning for forest investigation.” *Forest Ecosystems* 8: 1–15.
- Wang, Yunsheng, Matti Lehtomäki, Xinlian Liang, Jiri Pyörälä, Antero Kukko, Anttoni Jaakkola, Jingbin Liu, Ziyi Feng, Ruizhi Chen, and Juha Hyyppä. 2019. “Is field-measured tree height as reliable as believed—A comparison study of tree height estimates from field measurement, airborne laser scanning and terrestrial laser scanning in a boreal forest.” *IS-PRS journal of photogrammetry and remote sensing* 147: 132–145.
- Wang, Zhepei, Xin Zhou, Chao Xu, and Fei Gao. 2022. “Geometrically constrained trajectory optimization for multicopters.” *IEEE Transactions on Robotics* 38 (5): 3259–3278. <https://doi.org/doi.org/10.1109/TRO.2022.3160022>.
- Wieser, Martin, Gottfried Mandlbürger, Markus Hollaus, Johannes Otepka, Philipp Glira, and Norbert Pfeifer. 2017. “A case study of UAS borne laser scanning for measurement of tree stem diameter.” *Remote Sensing* 9 (11): 1154.
- Xu, Wei, Yixi Cai, Dongjiao He, Jiarong Lin, and Fu Zhang. 2022. “FAST-LIO2: Fast Direct LiDAR-Inertial Odometry.” *IEEE Transactions on Robotics* 38 (4): 2053–2073. <https://doi.org/10.1109/TRO.2022.3141876>.
- Xu, Zhuangzhi, Xin Shen, and Lin Cao. 2023. “Extraction of Forest Structural Parameters by the Comparison of Structure from Motion (SfM) and Backpack Laser Scanning (BLS) Point Clouds.” *Remote Sensing* 15: 2144. <https://doi.org/10.3390/rs15082144>.
- Ye, Ning, Louise van Leeuwen, and Panagiotis Nyktas. 2019. “Analysing the potential of UAV point cloud as input in quantitative structure modelling for assessment of woody biomass of single trees.” *International Journal of Applied Earth Observation and Geoinformation* 81: 47–57.
- Zhang, Zichao, and Davide Scaramuzza. 2018. “A Tutorial on Quantitative Trajectory Evaluation for Visual(-Inertial) Odometry.” In *2018 IEEE/RSJ International Conference on Intelligent Robots and Systems (IROS)*, 7244–7251.
- Zhou, Boyu, Hao Xu, and Shaojie Shen. 2023. “RACER: Rapid Collaborative Exploration With a Decentralized Multi-UAV System.” *IEEE Transactions on Robotics* 39 (3): 1816–1835. <https://doi.org/10.1109/TRO.2023.3236945>.
- Zhou, Boyu, Yichen Zhang, Xinyi Chen, and Shaojie Shen. 2021a. “FUEL: Fast UAV Exploration Using Incremental Frontier Structure and Hierarchical Planning.” *IEEE Robotics and Automation Letters* 6 (2): 779–786. <https://doi.org/10.1109/LRA.2021.3051563>.
- Zhou, Xin, Zhepei Wang, Hongkai Ye, Chao Xu, and Fei Gao. 2021b. “EGO-Planner: An ESDF-Free Gradient-Based Local Planner for Quadrotors.” *IEEE Robotics and Automation Letters* 6 (2): 478–485. <https://doi.org/10.1109/LRA.2020.3047728>.
- Zhou, Xin, Xiangyong Wen, Zhepei Wang, Yuman Gao, Haojia Li, Qianhao Wang, Tiankai Yang, et al. 2022. “Swarm of micro flying robots in the wild.” *Science Robotics* 7 (66): eabm5954. <https://doi.org/doi.org/10.1126/scirobotics.abm5954>.
- ZJU FAST Lab Team. 2022a. “EGO-Planner-v2.” Zhejiang University. <https://github.com/ZJU-FAST-Lab/EGO-Planner-v2>.

ZJU FAST Lab Team. 2022b. "px4ctrl." Zhejiang University. [https://github.com/ZJU-FAST-Lab/Fast-Drone-250/tree/master/src/realflight\\_modules/px4ctrl](https://github.com/ZJU-FAST-Lab/Fast-Drone-250/tree/master/src/realflight_modules/px4ctrl).